AD_____

Award Number: W81XWH-10-1-0560

TITLE: Understanding the Potential Role of Circulating Tumor Cells in Prostate Cancer Metastasis

PRINCIPAL INVESTIGATOR: Ajay Shah, Ph.D.

CONTRACTING ORGANIZATION: Massachusetts General Hospital
Boston, MA 02114-2621

REPORT DATE: August 2012

TYPE OF REPORT: Revised Annual Summary

PREPARED FOR: U.S. Army Medical Research and Materiel Command
Fort Detrick, Maryland 21702-5012

DISTRIBUTION STATEMENT: Approved for Public Release;
Distribution Unlimited

REPORT DOCUMENTATION PAGE

Form Approved
OMB No. 0704-0188

1. REPORT DATE	2. REPORT TYPE	3. DATES COVERED
August 2012	Revised Annual Summary	15 July 2010 – 14 July 2012

4. TITLE AND SUBTITLE

Understanding the Potential Role of Circulating Tumor Cells in Prostate Cancer Metastasis

5a. CONTRACT NUMBER

5b. GRANT NUMBER
W81XWH-10-1-0560

5c. PROGRAM ELEMENT NUMBER

6. AUTHOR(S)

Ajay Shah, Ph.D.

E-Mail: ajaymshah@gmail.com

5d. PROJECT NUMBER

5e. TASK NUMBER

5f. WORK UNIT NUMBER

7. PERFORMING ORGANIZATION NAME(S) AND ADDRESS(ES)

Massachusetts General Hospital
Boston, MA 02114-2621

8. PERFORMING ORGANIZATION REPORT NUMBER

9. SPONSORING / MONITORING AGENCY NAME(S) AND ADDRESS(ES)
U.S. Army Medical Research and Materiel Command
Fort Detrick, Maryland 21702-5012

10. SPONSOR/MONITOR'S ACRONYM(S)

11. SPONSOR/MONITOR'S REPORT NUMBER(S)

12. DISTRIBUTION / AVAILABILITY STATEMENT
Approved for Public Release; Distribution Unlimited

13. SUPPLEMENTARY NOTES

14. ABSTRACT

Major work performed during the period of performance included (1) development of a novel hydrogel system to enable the capture and release of specific cells from whole blood in microfluidic devices, as well as (2) the design of a new microfluidic cell isolation system that enables the antigen-dependent and antigen-independent isolation of circulating tumor cells from whole blood.

15. SUBJECT TERMS
None provided.

16. SECURITY CLASSIFICATION OF:			17. LIMITATION OF ABSTRACT	18. NUMBER OF PAGES	19a. NAME OF RESPONSIBLE PERSON
a. REPORT	b. ABSTRACT	c. THIS PAGE			USAMRMC
U	U	U	UU	35	19b. TELEPHONE NUMBER *(include area code)*

Table of Contents

Introduction

Metastasis, the spread and growth of tumor cells from the primary site to distant organs, is arguably the most devastating and deadly attribute of cancer, and is ultimately responsible for 90% of cancer-related deaths. Circulating tumor cells (CTCs) are exceedingly rare cells found in the whole blood of cancer patients which have the potential to serve as a 'blood biopsy'. The intricate characterization of these cells could result in an entire new class of therapies directly targeting metastasis.

Present technologies enable only a susbset of potential analyses to be conducted, principally due to sub-optimal cell isolation sensitivity, purity, throughput, or handling method. Towards this goal, two novel technologies to address the challenge of CTC isolation were developed during the performance of this award and are outlined in this report.

Second, we developed a novel cell sorting system that interrogates over 10 million individual events each second, resulting in a high throughput, ultra-efficient rare cell sorter that delivers enriched cells in a vial, readily compatible with virtually any downstream assay. This is the first system combining the high sensitivity and single cell resolution that is characteristic of FACS with the practicality of MACS at a throughput and specificity afforded by inertial focusing, enabling operation in both 'positive selection' and 'negative depletion' modes. We find greater than 90% cell isolation efficiencies with over 2.5 log depletion of contaminating WBCs. Furthermore, the system is applied to clinical patient samples, and proof-of-concept is demonstrated in a cohort of breast, lung and prostate patients.

Working in a negative depletion mode to isolate target cells in an unbiased fashion, we used the system to assess single putative CTCs isolated from an endogenous pancreatic mouse model for gene expression of tumor markers. Initial data confirms CTC heterogeneity at the single cell level, and positions us to move forward with single cell transcriptome sequencing, which may reveal a broad array of CTC phenotypes including metastatic precursors.

With regards to the training plan activities proposed in the supplementary SOW, 7 of the 8 tasks were completed (the exception being a course that was cancelled by the institution), and the PI successfully published 2 peer-reviewed publications in prestigious journals including *Analytical Chemistry* and *Science Translational Medicine*. The PI has since successfully defended his doctoral work at the Massachusetts Institute of Technology and received a PhD from MIT in June of 2012.

Body

Research Efforts:
The first technology, outlined in Aim 1 of the SOW focused on developing a release strategy for CTCs isolated using an antigen-based surface capture approach. Here, we build on affinity-based microfluidic cell capture platforms by developing sacrificial hydrogel coatings to enable the innocuous release of captured cells; we demonstrate that model CTCs captured from whole blood remain viable and proliferative following release and are compatible with downstream immunostaining and FISH analysis.

This technology is fully described in the following peer-reviewed publication, a copy of which is included in the appendix of this report:

> A. Shah, et. al. Biopolymer system for cell recovery from microfluidic cell capture devices. Anal Chem. 2012 Apr 17;84(8):3682-8. doi: 10.1021/ac300190j. Epub 2012 Apr 3.

Unfortunately, after evaluating a number of coating methodologies including spincoating, spraycoating, coating one side of the HB-chip device, and growing the hydrogel from the surface of the chip, we were unable to successfully develop a reliable, reproducible method to coat the HB-chip with the novel alginate coating. We determined that the HB-chip geometry was extremely sensitive to even small perturbations in surface properties, and as such, a coating approach was not feasible.

We therefore sought to develop an alternate CTC isolation strategy that was not dependent on cell-surface interactions. This novel cell sorting system interrogates over 10 million individual events each second, resulting in a high throughput, ultra-efficient rare cell sorter that delivers enriched cells in a vial, readily compatible with virtually any downstream assay – the end goal of the cell release work and critical to the tasks outlined in the SOW.

This is the first system combining the high sensitivity and single cell resolution that is characteristic of FACS with the practicality of MACS at a throughput and specificity afforded by inertial focusing, enabling operation in both 'positive selection' and 'negative depletion' modes. We find greater than 90% cell isolation efficiencies with over 2.5 log depletion of contaminating WBCs. Furthermore, the system was applied to clinical patient samples, and proof-of-concept is demonstrated in a cohort of breast, lung and prostate patients.

This technology is fully described in the following peer-reviewed publication, a copy of which is included in the appendix of this report:

> E. Ozkumur*, A. Shah*, et. al. Inertial focusing for tumor antigen-dependent and -independent sorting of rare circulating tumor cells. Sci Transl Med. 2013 Apr 3;5(179):179ra47. doi: 10.1126/scitranslmed.3005616.d * denotes equal contribution

Initial (unpublished) characterization of prostate CTCs isolated using this technology is presented below, using methods referenced in the publication. Here, we demonstrate the use of

'positive selection' for isolation of PSA+ PSMA+ CTCs (Figure 1) and we demonstrate that bulk qPCR analysis of cells isolated using 'negative depletion' from a prostate cancer patient demonstrates the presence of putative CTC markers at the RNA level when compared to a similarly processed healthy donor; PSA+ , PSMA+ and dual PSA+PSMA+ CTCs were identified in this sample by standard immunofluoresence. (Figure 2, Figure)

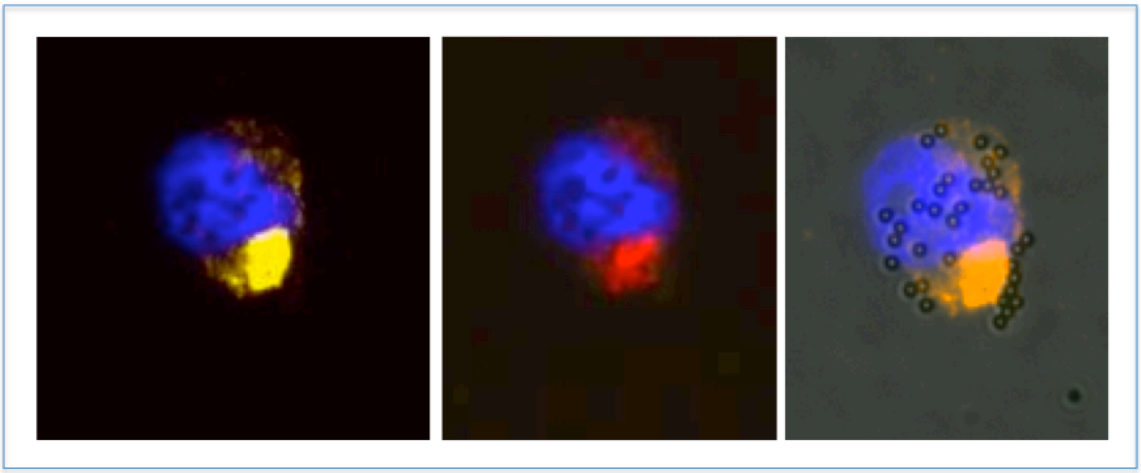

Figure 1. Example of a PSA+/PSMA+ CTC isolated using positive selection from a patient with metastatic prostate cancer. The sample was stained for DAPI (blue, all panels), PSMA (yellow, left) and PSA (red, center). The right panel shows co-localization of the PSA and PSMA signals in the cytoplasm, as well as demonstrating the presence of the EpCAM beads used for cell isolation.

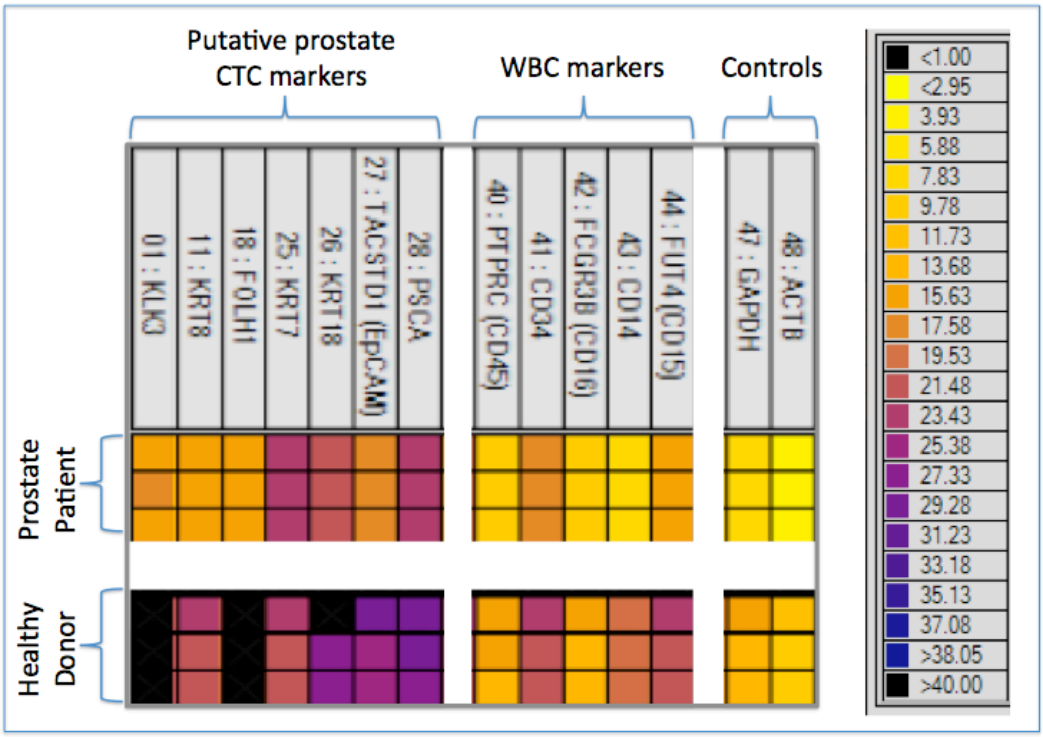

Figure 2. Fluidigm bulk qPCR analysis of negative depletion product enriched from a prostate patient's whole blood. This analysis demonstrates increased gene expression for CTC markers

when compared to a similarly processed healthy donor, particularly for PSA (KLK3) and PSMA (FOLH1).

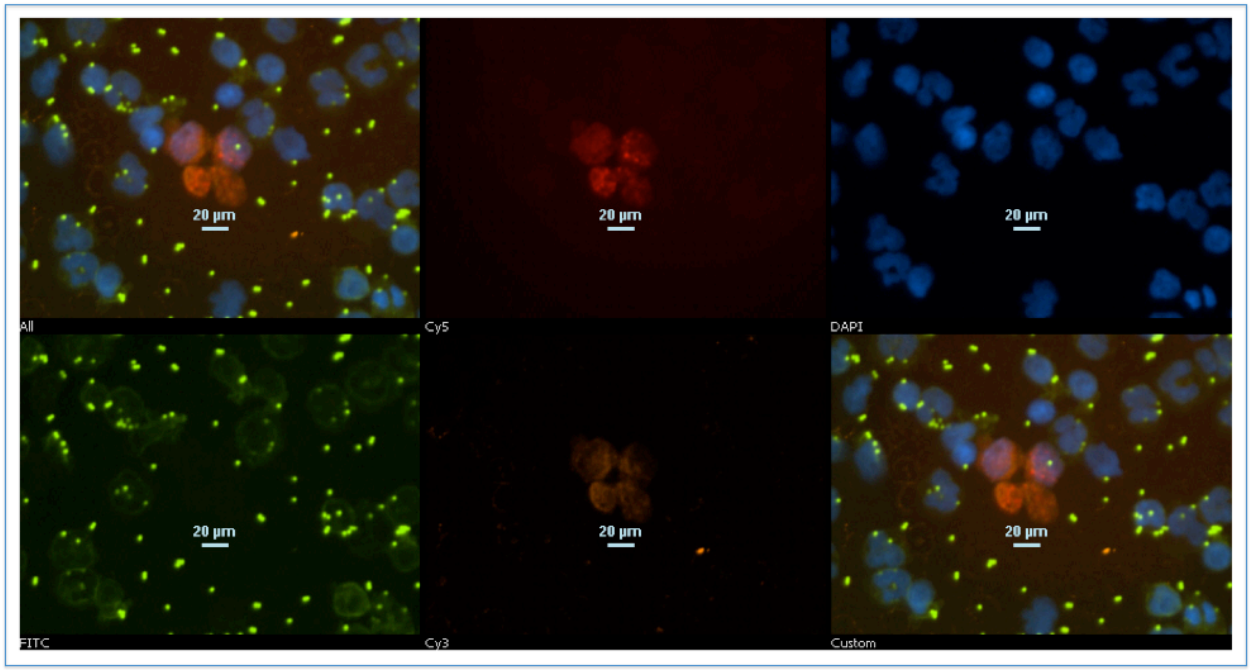

Figure 3. Immunoflourescent confirmation of prostate CTCs from the patient sample presented in Figure . Stains include DAPI (blue), PSA (Cy5), PSMA (Cy3), CD45 (FITC). Note that the punctate FITC staining is due to inadvertent labeling of free magnetic beads with the fluorescent secondary antibody.

Training Efforts:

Information relating to the 8 training tasks outlined in the supplemental SOW is included below.

- Task 1: Enroll in coursework relevant to prostate cancer biology
  - Completed throughout doctoral studies.

- Task 2: Complete Introduction to Clinical Medicine, HST.201 and HST.202
  - Both courses completed in January and June 2011.

- Task 3: Complete Introduction to Clinical Medicine, HST.203, with a focus on clinical treatment of prostate cancer
  - This course was cancelled by MIT, and as such not undertaken.

- Task 4: Present relevant data based on my work studying CTCs from prostate cancer patients at group meetings
  - Competed on a biweekly basis

- Task 5: Meet individually with Drs. Haber and Toner on a biweekly basis
  - Completed. As graduate work progressed, meetings were held on a weekly basis with both Drs. Haber and Toner to ensure continuity.

- Task 6: Formally present at the Center for Engineering in Medicine and the Cancer Center
    - Completed. Presentations were made to both groups in early 2012.

- Task 7: Publish results in refereed academic journal
    - Completed: Two first-author manuscripts were published in *Analytical Chemistry* and *Science Translational Medicine.* Additionally, the PI contributed to, and was named as an author on, publications in *Science* and *PNAS.*

- Task 8: Present results at national academic meetings
    - Completed: The work was accepted for presentation as a poster at the CDMRP ImPACT meeting and an oral presentation at the 2012 Annual BMES Conference.

Key Research Accomplishments:

- A photo-crosslinked, biofunctional, enzymatically-degradable, hyrdrogel coating for microfluidic devices that enabled specific cell capture and release from whole blood was developed and validated

- A novel magnetic bead based system for isolation of CTCs from whole blood was developed and characterized. Functioning in both positive selection and negative depletion modes, this method demonstrates high recovery and purification of rare cells.

- The cell isolation technology was applied to samples from prostate cancer patients and successful isolation of these cells and downstream solution-based biologloical assays were performed, demonstrating the power of this technology to enable further biological study of prostate CTCs.

Key Training Accomplishments:

- 2 first author manuscripts published in *Analytical Chemistry* and *Science Translational Medicine*
- Presentations made at national academic meetings
- PhD awarded from MIT to Ajay M. Shah

- **Reportable Outcomes:**
- Manuscripts published:
    - A. Shah, et. al. Biopolymer system for cell recovery from microfluidic cell capture devices. Anal Chem. 2012 Apr 17;84(8):3682-8. doi: 10.1021/ac300190j. Epub 2012 Apr 3.
    - E. Ozkumur*, A. Shah*, et. al. Inertial focusing for tumor antigen-dependent and -independent sorting of rare circulating tumor cells. Sci Transl Med. 2013 Apr 3;5(179):179ra47. doi: 10.1126/scitranslmed.3005616.d

- Degrees obtained: PhD awarded to Ajay M. Shah by the Massachusetts Institute of Technology (MIT) in June 2012

- Employment obtained: As a result of expertise gained in microfluidics, cell analysis technologies, and oncology, the PI obtained a senior position at a early stage startup company.

Conclusions:

In this work, two novel technologies are presented with the overall aim of enabling detailed characterization of circulating tumor cells with an array of immunophenotyping and molecular analysis tools.

Summary of contributions

Initially, we developed a novel biomaterial coating for microfluidic cell capture devices. As demonstrated, this coating facilitates cell capture with an efficiency comparable to standard chemistries, while enabling the release of virtually all captured cells upon degradation of the sacrificial coating. Importantly, the backbone degradation mechanism is innocuous to mammalian cells, and is demonstrated to have no effect on cell viability or proliferative potential. By dissolving the entire coating rather than targeting particular linkages, both specific (antibody-antigen) and non-specific (electrostatic) cell-surface linkages are cleaved, resulting in highly efficient release of captured cells. This study clearly demonstrated the utility of sacrificial coatings to enable the release of immunoaffinity captured cells from microfluidic cell capture devices.

Second, we developed an entirely new CTC isolation technology, known as the iChip system. This system integrates three microfluidic components – lossless debulking of whole blood, precise cell positioning using inertial forces, and highly sensitive magnetophoresis. As demonstrated, this system can be used for either positive selection (with > 90% yield of low EpCAM expressing PC3-9 cells) or negative depletion (> 90% yield of ultra-low EpCAM expressing LBX1 cells). The enriched CTCs are collected in solution, and in the case of negatively enriched cells, free of any bound labels; this makes them readily compatible with a wide array of downstream assays. In an initial cohort of breast, prostate and lung patients, we are able to readily indentify CTCs using standard immunofluoresence methods and molecular profiling. Furthermore, review of papanicalaou stained samples by a board-certified cytopathologist revealed ‘suspicious’ and ‘aberrant’ cells likely of tumorigenic origin. Together, this initial data validates the functionality of the MIMICS system for CTC isolation from a clinical cohort; it further demonstrates the potential for highly sensitive, solution-based cell isolation to enable new downstream analyses which were previously technically limited. Most compelling is the development of a robust, sensitive ‘negative depletion’ approach to enable near lossless isolation of non-hematopoietic cell populations from whole blood, as this has the potential to reveal previously unstudied subpopulations of CTCs.

Recommendations for future work

Sacrificial coatings for the release of immunoaffinity captured cells

The efforts towards release of immuno-affinity captured cells presented in this thesis clearly motivate the use of a sacrificial layer approach. While the work shown encompasses biomaterial development and validation, the key step needed to enable CTC capture and release is integrating the coating with the three-dimensional HB-chip micro-architecture in a conformal fashion. This is critical, as preservation of the microchip architecture is necessary to enable efficient rare cell capture.

Alternative approaches to forming sacrificial coatings (beyond those evaluated in this project) could be considered, as they may be more amenable to conformal coating. For instance, layer-by-layer (LBL) deposition is a well established method to form conformal hydrogels. By successively depositing polymers with opposing charges, a hydrogel may be formed as electrostatic forces hold the polymer layers together. Importantly, each layer is 'self-terminating' and thus conformal coatings may be easily formed. Another strategy to consider would be polymer vapor deposition; hydrogels formed using this approach have been demonstrated to conformally coat complex geometries. Key to the success of either of these approaches will be the selection of polymers and crosslinkers with rapidly degradable moieties to enable dissolution and cell release.

The iChip cell isolation system

The iChip system presented in this thesis represents a notable improvement in microfluidic immuno-based cell isolation. While promising, the system needs to be further validated using a larger clinical cohort and with direct comparisons to other CTC enrichment strategies, such as the HB-Chip and the CellSearch system. Coupling the system with downstream lossless cell handling and plating methods would notably improve the utility of the technology. Further improvements should focus on advancing both the cell capture efficiency and purity. For 'positive selection', this may be achieved by exploring a variety of capture moieties beyond EpCAM. These could include antibodies or aptamers against disease-specific targets such as EGFR (lung cancer), HER2 (breast cancer), or PSMA (prostate cancer). Positive selection would also benefit from increases in purity through targeted removal of contaminating WBCs; possible approaches could include surface immuno-affinity capture or antibody directed photolysis.

Achieving another order of magnitude of purification in the 'negative depletion' mode would be an important advancement of the technology; this is imperative to enable molecular analyses of samples enriched in this manner. Multiple avenues exist to achieve this goal, including fluidic, magnetic and reagent enhancements. Based on the mathematical model presented in the publication, a minimum of 6-8 beads are needed to deflect white blood cells; this calculation, along with the probabilistic distribution of bead-cell interactions during the labeling process, suggests that many of the undeflected WBCs are labeled with magnetic beads, but in numbers below the deflection threshold. These cells could be magnetically removed from the sample using a secondary purification channel in which the residence time was increased by expanding the channel cross-section and therefore decreasing the magnetic load needed to deflect. As this approach would disrupt cell focusing, the WBCs would need to be deflected not to a side stream, but to the bottom of the channel, where they could be magnetically held in place while the target cells continued to the outlet. Another strategy to deplete cells with low levels of bead labeling would be to create a high-gradient magnetic field in the deflection region, thereby decreasing the magnetic load needed to deflect a cell to the side of the channel in the given residence time. High gradient fields have been commonly used in bulk cell isolation technologies, and have recently been integrated into microfluidic circuits; the major obstacle is the complexity of patterning and aligning magnetizable materials at the microscale. The third tactic that could be taken to improve the purity of the negative depletion product centers on modulating the reagents. While the 1 micron magnetic beads used here have a large magnetic moment, once a bead is bound to an antigen, surrounding antigens are sterically blocked from binding to additional beads; given that WBCs express millions of copies of CD45 on their surface, the effective copy

number is dramatically reduced due to this steric hindrance. Therefore, using much smaller (~50 nm) highly magnetizable particles, which would not block surrounding antigens, has the potential to increase the overall magnetic loading on a cell. Finally, it should be noted that while the vast majority of non-tumor cells found in whole blood express CD45 and CD15, there are other rare cell populations that exist in blood and lack these antigens, such as megakaryocytes and circulating endothelial progenitor cells; specific targeting of these cell populations should be considered. Similarly, should characterization of the undepleted WBCs reveal a specific subpopulation of leukocytes, direct targeting of this subpopulation through specific antigens would be warranted.

References

A. Shah, et. al. Biopolymer system for cell recovery from microfluidic cell capture devices. Anal Chem. 2012 Apr 17;84(8):3682-8. doi: 10.1021/ac300190j. Epub 2012 Apr 3.

E. Ozkumur*, A. Shah*, et. al. Inertial focusing for tumor antigen-dependent and -independent sorting of rare circulating tumor cells. Sci Transl Med. 2013 Apr 3;5(179):179ra47. doi: 10.1126/scitranslmed.3005616.d * denotes equal contribution

Appendix

Attached are the publications previously referenced.

analytical chemistry

Article

pubs.acs.org/ac

Biopolymer System for Cell Recovery from Microfluidic Cell Capture Devices

Ajay M. Shah,[†,§] Min Yu,[‡,#] Zev Nakamura,[‡] Jordan Ciciliano,[‡] Matthew Ulman,[‡] Kenneth Kotz,[§,⊥,▽] Shannon L. Stott,[§,⊥,▽] Shyamala Maheswaran,[‡,⊥] Daniel A. Haber,[‡,∥,#] and Mehmet Toner*[,§,⊥,▽]

[†]Harvard-MIT Division of Health Sciences and Technology, Massachussets Institute of Technology, Cambridge, Massachusetts 02139, United States

[‡]Cancer Center, [§]Center for Engineering in Medicine, [∥]Departments of Medicine and [⊥]Surgery, Massachussets General Hospital and Harvard Medical School, Boston, Massachusetts 02114, United States

[#]Howard Hughes Medical Institute, Chevy Chase, Maryland 20815, United States

[▽]Shriners Hospital for Children, Boston, Massachusetts 02114, United States

Supporting Information

ABSTRACT: Microfluidic systems for affinity-based cell isolation have emerged as a promising approach for the isolation of specific cells from complex matrices (i.e., circulating tumor cells in whole blood). However, these technologies remain limited by the lack of reliable methods for the innocuous recovery of surface captured cells. Here, we present a biofunctional sacrificial hydrogel coating for microfluidic chips that enables the highly efficient release of isolated cells (99% ± 1%) following gel dissolution. This covalently cross-linked alginate biopolymer system is stable in a wide variety of physiologic solutions (including EDTA treated whole blood) and may be rapidly degraded via backbone cleavage with alginate lyase. The capture and release of EpCAM expressing cancer cells using this approach was found to have no significant effect on cell viability or proliferative potential, and recovered cells were demonstrated to be compatible with downstream immunostaining and FISH analysis.

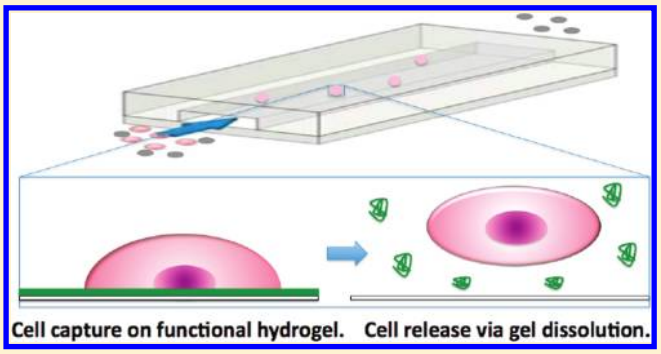

Continuous flow affinity-based microfluidic devices are emerging to fill an important niche in cell sorting.[1,2] These technologies focus on coating a surface with a capture moeity and then utilize microfluidic architectures to precisely control and maximize cell−ligand interactions.[3−5] The label-free nature of these techniques enables the isolation of cell populations from complex solutions (i.e., whole blood) with minimal or no preprocessing. This allows for the rapid isolation of a wide variety of clinically relevant cell types, ranging from exceedingly rare circulating tumor cells,[5] to CD4+ T cells,[6] to more prevalent neutrophils.[7,8] At present, only limited downstream analysis (most commonly, imaging-based approaches) may be conducted due to the inability to reliably elute viable cells from the microfluidic chips. For genetic analyses, mixed cell populations must be lysed on chip[9] and only limited amounts of material can be recovered, restricting the ability to do full genome wide studies of rare cell populations. Furthermore, the cells are unavailable for downstream purification, differentiation of complex subpopulations, single cell genomic analyses, or subsequent culture *in vitro* or in animal models.

Cells initially captured on immuno-affinity substrates via specific antibody−antigen binding are likely to form other nonspecific linkages with the surface over time. These nonspecific linkages may confound any molecular release mechanisms which cleave only specific antibody linkages. Potential approaches for the release of surface captured cells range from chemical methods such as gradient elution to mechanical approaches such as the application of high shear stress and the use of bubbles within capillary systems.[10,11] Both chemical and mechanical approaches have the potential to cause significant harm to the target cell populations. Even if cell integrity is preserved, the ability to extract phenotypic and functional information from target populations may be compromised as variations in chemical microenvironments and shear stress are known to cause significant changes in gene expression patterns.[12]

In limited studies, the combination of a proteolytic enzyme and surfactant enabled the release of captured cells for immediate enumeration;[13−15] the degradation of surface markers and potential membrane disruption due to the

Received: January 18, 2012
Accepted: March 9, 2012
Published: March 10, 2012

surfactant, however, may limit the feasibility of this approach for downstream biological analyses of target cells.

Phase-changing hydrogels, such as temperature[16] and UV sensitive gels,[17] have emerged as a potential method to regulate cell-surface interactions. Recently, Hatch et al.[18] demonstrated that ionically cross-linked hydrogels formed *in situ* enabled the capture, release, and FACS analysis of endothelial progenitor cells from heparinized whole blood. Notably, this study demonstrated the feasibility of a cation-cross-linked sacrificial hydrogel approach for microfluidic cell capture and release without enzymatic digestion of cell surface proteins. This system, while promising, has a limited scope of use as it cannot be used in conjunction with common anticoagulation strategies that work on the principle of calcium chelation (EDTA, citrates, etc.).[19,20] Furthermore, during cell release, target cells are exposed to nonphysiologic levels of calcium chelating agents which may initiate unwanted signaling cascades within the target cells and have the potential to alter the observed cell phenotype and proliferation state.[21−23]

Here we present a photo-cross-linked, degradable biopolymer coating that enables the gentle, efficient release of antibody-captured cells from microfluidic devices. Our coatings are of controlled thickness, stable for extended periods of time, and may be used with a wide variety of buffers and physiological fluids (including EDTA-treated whole blood). The release mechanism we employ is the backbone degradation of our alginate biopolymer by a specific bacterial enzyme (alginate lyase) which is commonly used in combination with cell cultures.[24−26] We further demonstrate that released cells are viable and proliferative.

EXPERIMENTAL SECTION

Alginate Modification. Pharmaceutical grade alginate (Pronova UP MVG, Novamatrix, Norway, 60% guluronate, 40% mannuronate) was modified with both N-(3-aminopropyl)methacrylamide HCl (Polysciences 21200-5) and biotin hydrazide (Sigma B7639) using standard carbodiimide chemistry in a single reaction. Briefly, alginate was prepared at 1% by weight in MES buffer, pH = 6.0. Per 100 mL of alginate solution, 0−159 mg of biotin hydrazide, 225.63 mg of methacrylamide, 721 mg of 1-ethyl-3-[3-dimethylaminopropyl]carbodiimide hydrochloride (EDC, Pierce 22980), and 408 mg of hydroxysulfosuccinimide (Sulfo-NHS, Pierce 24510) were added and reacted for 3 h, after which time the solution was dialyzed against dH2O for 48 h and lyophilized. Alginate was reconstituted at 2% in dH2O prior to use.

Hydrogel Formation. Substrates were pretreated with a molecular-scale layer of alginate by first aminating the surface with a solution of 3-aminopropyltriethoxysilane (Pierce 80370, in 95% ethanol, pH = 5.0 for five minutes) followed by reacting the amine-surface overnight with a dilute alginate solution (0.1% in MES, pH = 6.0) containing 3.73 g of EDC and 2.11 g of Sulfo-NHS per 100 mL. Substrates were then rinsed and dried prior to spincoating. Alginate solutions were spun (spincoater WS-650SZ-6NPP/LITE, Laurel Technologies) at 3000 rpm for 30 s to control gel thickness, unless otherwise noted. Gels were then cross-linked using a 250 mM calcium chloride spray, followed by incubation in a 2.5 mM calcium solution, addition of the photoinitiator irgacure 2959 (Ciba Specialty Chemicals) (0.25%) to the solution, and then photo-cross-linking in a nitrogen environment for 10 min using a 365 nm UV lamp (UVP XX-15-BLB). Following cross-linking, the gels were washed to remove calcium and dried prior to use.

Patterning and Functionalizing Gels Inside Simple Microfluidic Geometries. Gels were spatially templated onto ultraclean glass slides (Thermo C22−5128-M20) by first applying a laser-cut elastomeric stencil in the shape of the microchannel on top of the glass prior to hydrogel formation. Following gel formation as described above, the stencil was removed, and a PDMS microchannel was plasma treated for 30 s (ElectroTechnic Products BD-20) and bonded around the hydrogel.[6] The PDMS microchannels used in this study were rectangular chambers 50 μm tall, 4 mm wide, and 50 mm long, fabricated using standard soft-lithography techniques.[27] The channels were flushed with PBS (rehydrating the gels), blocked in a 1% BSA solution for a minimum of 30 min (blocking the gel and PDMS walls), and functionalized with neutravidin (Pierce 31000, 50 μg/mL in 1% BSA) for 45 min. The channels were rinsed with PBS and incubated with a biotinylated anti-EpCAM antibody (R&D Systems BAF960, 20 μg/mL in 1% BSA for 45 min) when used for cell capture. In this model system, only the bottom surface of the channel was coated with the hydrogel, limiting the available area for cell binding.

Hydrogel Characterization. Hydrogel thickness was measured using a noncontact profilometer (Olympus LEXT OLS3100) after films were formed and dried. To characterize gel dissolution, 50 nm green fluorescent beads (Duke Scientific G50) were mixed into the alginate solution prior to gelation and thus impregnated in the resulting hydrogel; as the gel dissolved, beads were released and cleared away and the decrease in fluorescent signal intensity was monitored using time-lapse imaging. Initial steady-state intensity measurements were taken before treating the gel with alginate lyase at a particular concentration, and a final steady-state measurement was taken once the gel had fully degraded; these values were treated as 100% (initial) and 0% (final) relative intensities. For the control condition (0 μg/mL alginate lyase) all intensites were compared to the initial steady-state, as the gel did not degrade; the slight drop in intensity was observed to be caused by photobleaching of the sample by comparing the intensity of the gel immediately adjacent to exposed field of view. The experimental samples were observed to rapidly degrade, and so no notable photobleaching was observed.

Relative biofunctionality was measured using a sandwich assay in which the biotin incorporated into the hydrogel was coupled with neutravidin, rinsed with PBS, and then followed by a fluorescent biotinylated protein (biotin R-PE, 20 μg/mL for 45 min in 1% BSA, Life Tecnologies). The 'standard chemistry' is a silane-based coupling chemistry used in our laboratory to functionalize microfluidic devices with neutravidin; it was followed by the same biotin R-PE solution to assay the biotinylated protein binding capacity of the surface.[1]

Cell Capture, Release, and Recovery. Cell capture and release was characterized using both a prostate cancer (PC3) and breast cancer (SKBR3) cell line. All cell lines were obtained from ATCC and cultured in accordance with their recommendations.

The relative cell capture efficiency was evaluated by patterning gels in 10 × 10 mm squares and functionalizing with the anti-EpCAM antibody as described. PC3s in PBS buffer were then spotted onto the areas in a static capture assay to compare the relative cell capture potential of the functional alginate coatings as compared to the standard chemistry (positive control, set to 100%) and nonfunctional alginate

dx.doi.org/10.1021/ac300190j | *Anal. Chem.* 2012, 84, 3682−3688

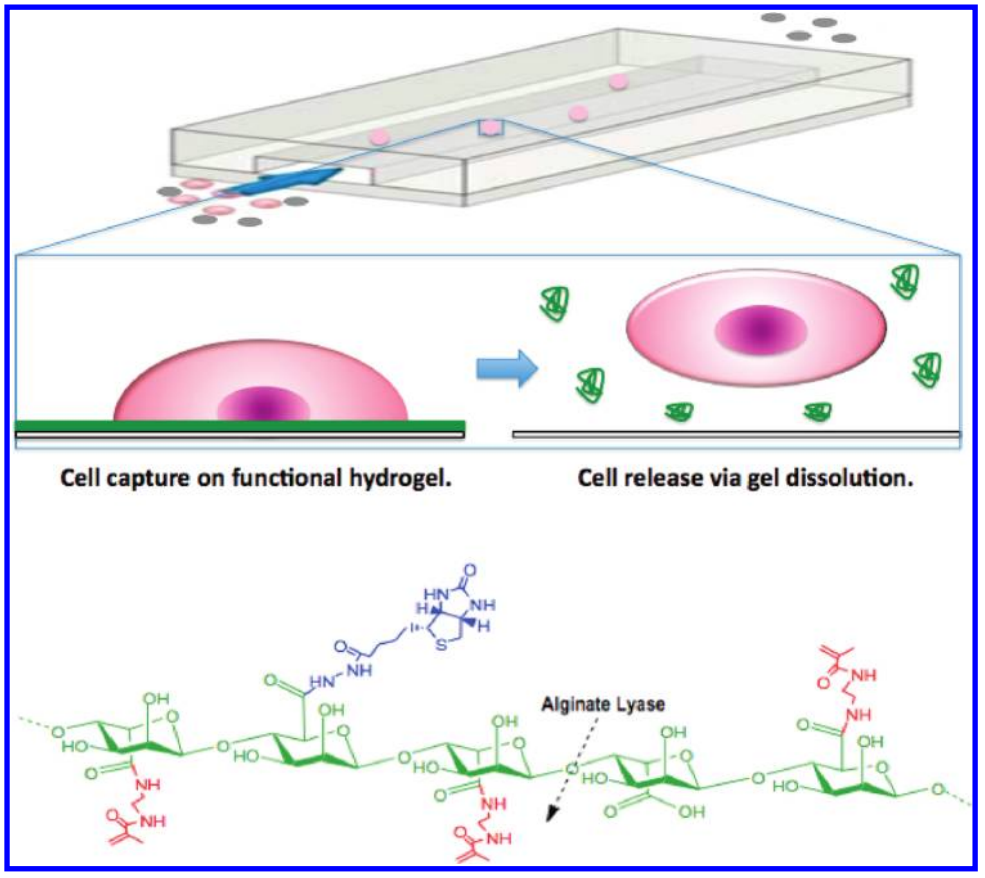

Figure 1. Sacrificial hydrogel coatings may be a compelling strategy for cell release from microfluidic devices, as they will release both specific and nonspecific cell-surface linkages. Here, we developed an alginate (green) biopolymer system which may be covalently cross-linked using methacryl groups (red) and biofunctionalized using biotin moieties incorporated in the base material (blue). The gel dissolution and subsequent cell release may be achieved by brief exposure to the bacterial enzyme alginate lyase which cleaves the backbone of the biopolymer.

(negative control). Following a brief incubation period, unbound cells were removed by gently washing the area with PBS. Cells were counted before and after washing to determine capture efficiency. This static assay evaluates the effect of surface ligand presentation on cell capture efficiency, separate from the effects of the microfluidic geometry. Together, these two parameters determine cell capture efficiency in affinity-based microfluidic cell isolation devices.

To evaluate performance of the hydrogel system for cell release and recovery efficiency, a model system was employed; briefly, PC3s were spiked into whole blood (10^6 cells/mL, notably higher than the CTC load found in patient samples) and captured in a microfluidic in which the bottom of the channel was coated with an anti-EpCAM functionalized hydrogel. After PC3s were captured (2 μL/min) and blood was rinsed out with PBS (20 μL/min), the channel was imaged and the total number of cells bound on the gel was counted. Alginate lyase (Sigma A1603, EC# 4.2.2.3, which targets the β-(1−4)-D-mannuronic bonds on the alginante backbone, 1 mg/mL in PBS) was then flowed through the channel (0.5 μL/min), releasing the cells which were recovered in an 8-well chamber slide and counted again. The ratio of cells recovered to cells captured was used to determine the recovery efficiency. The capture areas were reimaged to confirm recovery efficiency by verifying the mass balance.

Cell release was observed under a fluorescent microscope (Nikon TiE, Japan) by first prelabeling the cells with a dye (CellTracker Red, Life Technologies). Time-lapse images were taken every 200 ms and then analyzed using the tracking module within the manufacturer's software (Nikon Elements) to chart cell movement as a function of time during the release process.

Analysis of Released Cells. Recovered cell viability was measured using a standard live/dead fluorescent assay (Life Technologies L3224) and compared to control cells which were never introduced into the microfluidic system. Colony formation was measured by recovering PC3 cells from a spiked sample and then diluting the cells with culture medium to form a single cell culture environment. After 96 h, the number of colonies formed in the well were evaluated alongside the number of colonies formed from a similar number of control cells. HER2 amplified SKBR3 breast cancer cell line cells were captured and released in a similar fashion, cytospun, and then immunostained for the HER2 protein using a primary (Dako rabbit α-Erb2 A0485) secondary (Alexa Fluor 488 donkey α-rabbit, Life Technologies) antibody staining approach. Released SKBR3 cells were also probed with HER2 and centromere FISH probes using standard methods. In brief, released cells were cytospun and fixed with methanol-acetic acid (3:1), washed with 2X SSC, and dehydrated in an ascending series of ethanol, and a HER2/CEP-17 probe mix was added. DNA was then denatured at 75 °C and hybridized at 37 °C for 20 h, and posthybridization washes were performed in 0.4X SSC/0.3% NP-40 at 72 °C for 2 min and 2X SSC/0.1% NP-40 at room temp for 30 s. The samples were counterstained with mounting medium containing DAPI and imaged at 60X.

dx.doi.org/10.1021/ac300190j | *Anal. Chem.* 2012, 84, 3682−3688

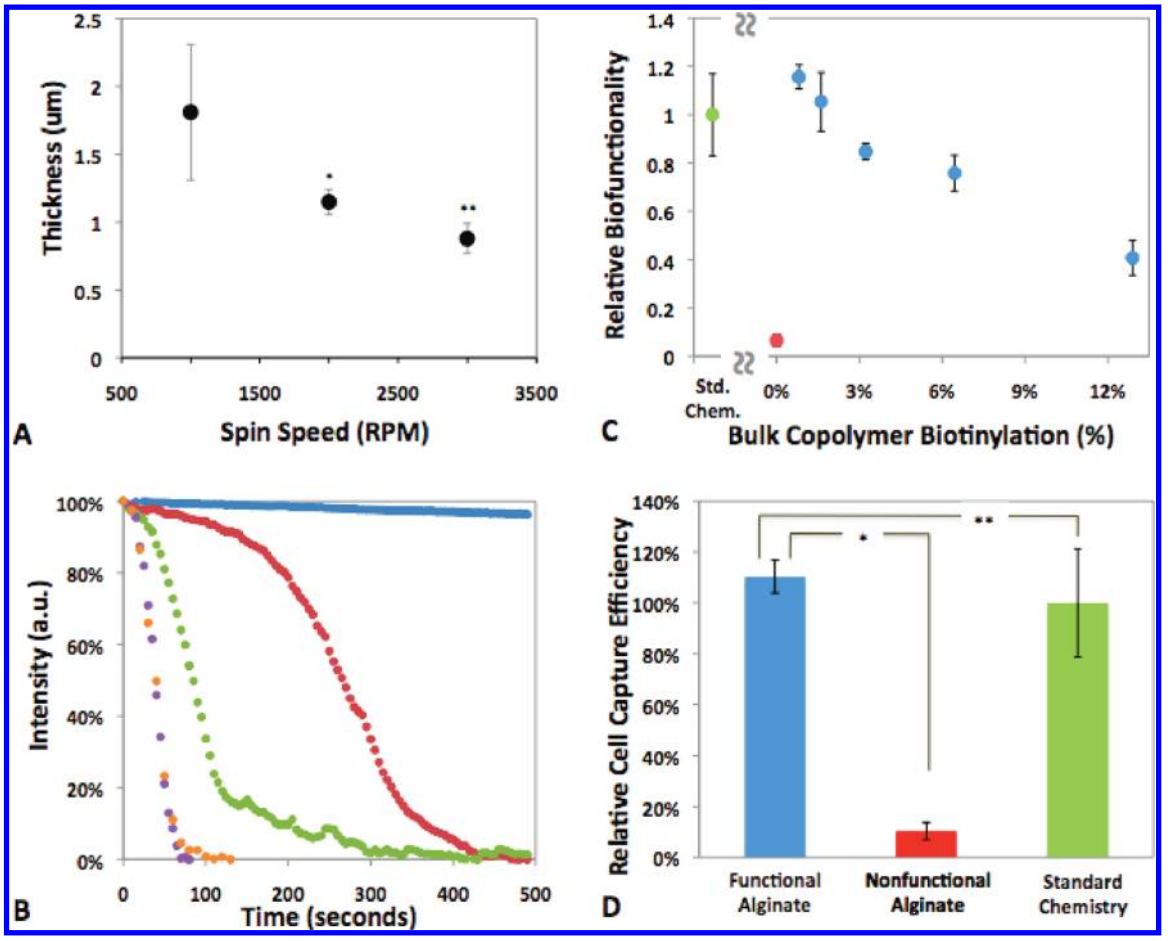

Figure 2. Alginate hydrogels were formed with (A) micrometer-scale thickness using a spincoating process (* $p = 0.017$; ** $p < 0.001$). (B) Upon treatment with alginate lyase at various concentrations (50 (red), 100 (green), 250 (purple), 1000 (orange) μg/mL, control PBS (blue)), photo-cross-linked hydrogels rapidly degraded in a dose-dependent fashion. Gels were (C) functionalized using gel-bound biotins, and an inverse trend between bulk biotin density and functionality was observed. A static cell capture assay (D) demonstrated that the functional material (blue) captured cells with an efficiency comparable (* indicates $p = 0.45$) to standard surface modification approaches (green), while nonfunctional gels (red) resisted physisorbtion of capture molecules and nonspecific cell binding (** indicates $p < 0.001$).

RESULTS AND DISCUSSION

Hydrogel Development and Characterization. Carboxyl groups on pharmaceutical grade alginate were modified using standard carbodiimide chemistry to present both methacryl groups (65% theoretical derivitization) and biotin moieties (0–12% theoretical derivitization) (Figure 1). The methacryl groups covalently cross-link the alginate to form a stable hydrogel, and the biotin imparts the bulk material with a ligand for further biofunctionalization. Conjugation was confirmed and quantified using proton NMR and HABA (4′-hydroxyazobenzene-2-carboxylic acid) assays, respectively (SI). As the microfluidic geometry of the channel is critical to maintaining the appropriate shear stress for cell capture, the thickness and roughness of the alginate layer was carefully controlled using spin-coating techniques to produce films in the submicrometer regime that would not affect overall channel fluidics (Figure 2A). The films were photo-cross-linked to form a hydrogel which was stable in the presence of calcium-chelating anticoagulants (i.e., EDTA) but could be rapidly degraded with the addition of alginate lyase (Figure 2B).

To ensure optimal ligand accessibility, a nanopatterning approach was employed similar to that developed by Comisar et al.[28,29] Here, highly biotinylated alginates (86 biotins per chain) were mixed in solution with nonbiotinylated ('blank') alginates. These biotinylated alginate chains coil in solution to form nanoislands of functionality spaced apart by blank alginates.[29] Optimal island density was studied by varying the ratio of biotinylated chains to blank chains in the copolymer preparation; neutravidin was used to cross-link the gel bound biotins with a biotinylated capture ligand, thereby presenting the capture ligand on the surface. This approach demonstrated an inverse trend in which lower bulk average biotin density in the gel correlated with higher ligand presentation (Figure 2C). Ligand presentation equivalent to that achieved with the silane-based chemistry commonly employed within microfluidic devices[1,4] ("standard chemistry") was realized with 5 to 10 bulk average biotins (Figure 2C). Static cell capture experiments validated the ligand presentation results; gels functionalized with an anti-EpCAM antibody captured EpCAM expressing prostate cancer cells at a comparable efficiency to that of the standard chemistry (Figure 2D).

Release and Characterization of Isolated Cells. To convey the gentle nature of the cell release process, a typical captured cell was imaged during the release process and the position of the cell was tracked over time (Figure 3). These data demonstrate how, as the gel is degraded, a captured cell (3A) first gradually detaches from the substrate, (3B) then moves slowly along the surface (3C) before being caught up in

dx.doi.org/10.1021/ac300190j | Anal. Chem. 2012, 84, 3682–3688

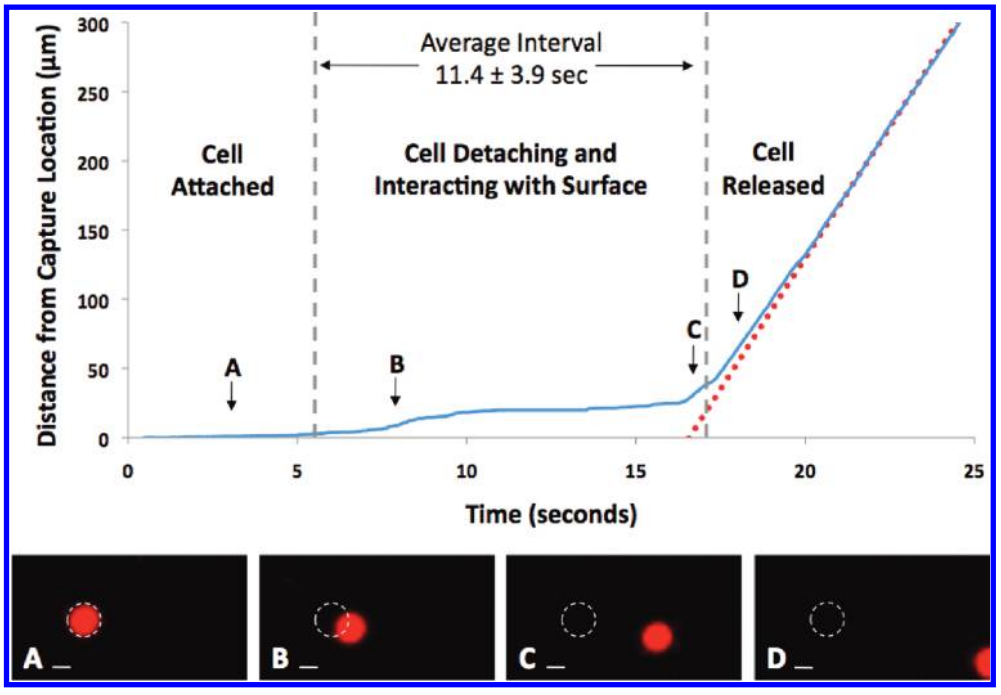

Figure 3. Cells from a prostate cancer cell line were spiked into whole blood, captured on an anti-EpCAM functionalized alginate gel, and released by dissolving the gel with alginate lyase. The progression of a typical cell during the release process (blue) was tracked using automated image processing software. Images A-D show the cell at various stages of the release process and mark the initial location of the cell with a white dashed circle. This series demonstrates the gentle nature of the release process as the cell starts (A) attached, then (B) slowly detaches and (C) travels along the surface until (D) it enters the free flow stream, now traveling at the average bulk velocity of the fluid in the channel (red dotted line). Scale bars are 10 μm. Cells (n = 15) from 3 different gels were tracked during release to determine the average interval between initial movement to final release.

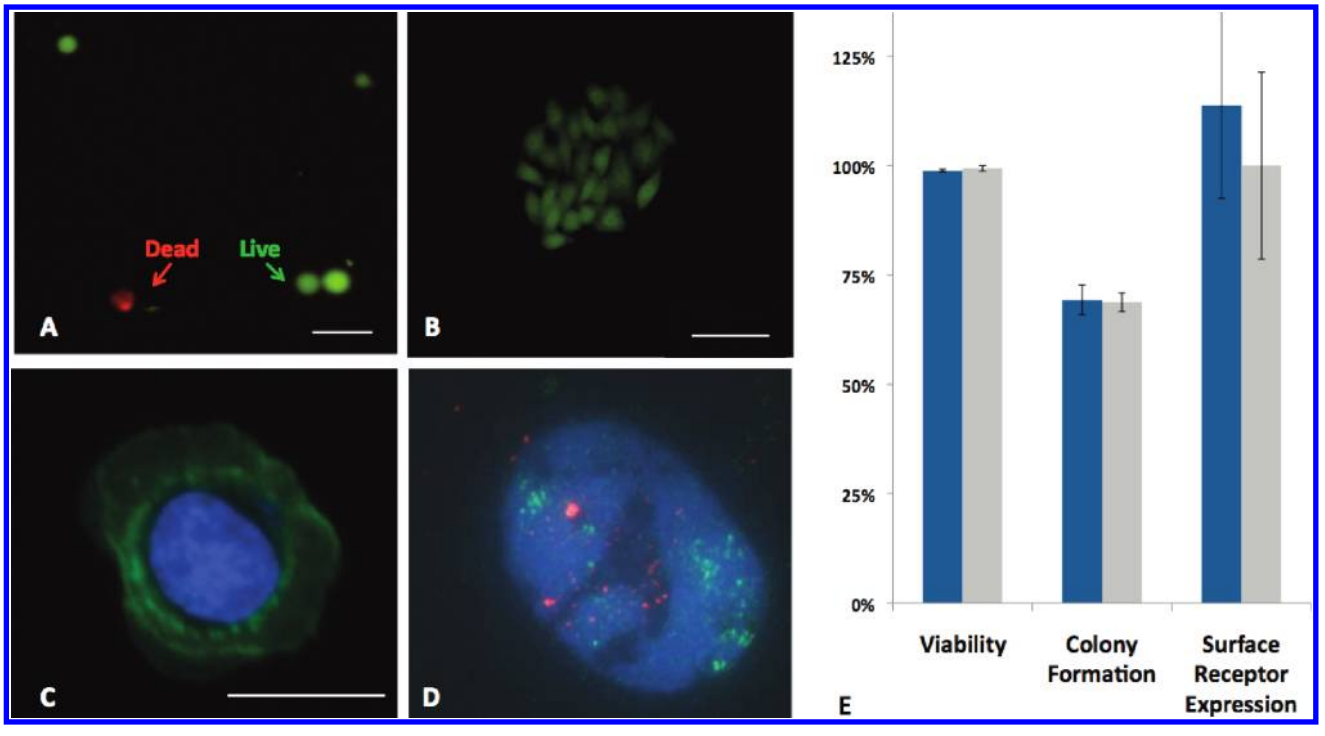

Figure 4. Released cells were evaluated for (A) viability using a fluorescent LIVE (green)/DEAD (red) assay and (B) colony formation; scale bars are 50 μm. Released cells were found to be compatible with downstream (C) immunostaining of cell surface receptors (shown here is HER2 expression in a released cell in green, counterstained with DAPI nuclear staining in blue; 20 μm scale bar). (D) FISH analysis was also feasible as shown here in a released HER2 (green probe) amplified breast cancer cell; the control probe is shown in red. (E) Released cells (blue bars) were found to have comparable viability (98.9% ± 0.3% vs 99.4% ± 0.6%), rates of colony formation from single cells (69.3% ± 3.4% vs 68.8% ± 2.2%), and relative surface receptor expression (113.8% ± 21.2% vs 100% ± 21.3%) when compared to control cells (gray bars) maintained in the appropriate cell culture medium (p > 0.05).

dx.doi.org/10.1021/ac300190j | *Anal. Chem.* 2012, 84, 3682−3688

the flow stream which moves it downstream at the bulk fluid velocity. The efficiency of this cell release process was evaluated by directly quantifying cell capture, release, and recovery. This study demonstrated a 99% ± 1% release efficiency. Released cells were characterized for their viability (98.9% ± 0.3%) compared to control cells simply spiked into whole blood (99.4% ± 0.6%) and found to be unaffected (Figure 4A,E). Similarly, effects of the capture and release process on cell proliferation was studied by diluting released cells in culture medium and measuring the extent of single cell colony formation after 96 h (69.3% ± 3.4%) as compared to similar control cells (68.8% ± 2.2%) (Figure 4B,E). As an initial demonstration of the compatibility of the release technology with downstream biological assays, breast cancer cells harboring amplified HER2 genes were spiked into blood, captured, released, and evaluated using standard immunostaining and fluorescence in situ hybridization (FISH) techniques. Expression of the HER2 surface receptor was found to be comparable to control cells (113% ± 21.2% relative intensity) (Figure 4C,E). Furthermore, HER2 gene amplification is readily evident by FISH, illustrating the potential broad applicability of this cell release technology to enable standard molecular diagnostic applications in a variety of clinical specimens (Figure 4D).

CONCLUSION

The alginate biopolymer system presented here represents an important step forward in developing affinity-based cell capture surfaces as it enables gentle, efficient recovery of isolated cells without compromising their viability or proliferative potential. The critical followup of this work is the development of precisely controlled coating techniques for the integration of this materials approach with the complex microfluidic architectures used for rare cell isolation.[1,4,9,13] While existing technologies have demonstrated their clinical relvance, recovering these cells with high efficiency and in an unadulterated fashion will place them in the hands of molecular and cell biologists in a manner that is readily compatible with their arsenal of sophisticated tools, so that we may begin to further elucidate the roles of these cells in human biology.[30−32]

ASSOCIATED CONTENT

Supporting Information

Demonstration of alginate acrylation by NMR, characterization of alginate biotinylation using a modified HABA assay, and equilibrium swelling of gels with varying acrylation. This material is available free of charge via the Internet at http://pubs.acs.org.

AUTHOR INFORMATION

Corresponding Author

*Fax: (+1) 617 724 2999. E-mail: mtoner@hms.harvard.edu. Corresponding author address: 114 16th St, Charlestown, MA 02129.

Notes

The authors declare no competing financial interest.

ACKNOWLEDGMENTS

The authors thank Octavio Hurtado and Laura Libby for expert technical support and Dr. Sangeeta Bhatia for insightful conversations. This work was supported by Dream Team awards from the Prostate Cancer Foundation and Stand Up to Cancer (to D.A.H. and M.T.) and a Quantum Grant from the National Institute for Biomedical Imaging and Bioengineering (NIBIB) to M.T. A.M.S. is supported by a DOD PCRP predoctoral fellowship.

REFERENCES

(1) Nagrath, S.; Sequist, L. V.; Maheswaran, S.; Bell, D. W.; Irimia, D.; Ulkus, L.; Smith, M. R.; Kwak, E. L.; Digumarthy, S.; Muzikansky, A.; Ryan, P.; Balis, U. J.; Tompkins, R. G.; Haber, D. A.; Toner, M. *Nature* **2007**, *450*, 1235−1239.

(2) Evanko, D. *Nature Methods* **2008**, *5*, 124.

(3) Wang, S.; Liu, K.; Liu, J.; Yu, Z.; Xu, X.; Zhao, L.; Lee, T.; Lee, E. K.; Reiss, J.; Lee, Y.; Chung, L. W. K.; Huang, J.; Rettig, M.; Seligson, D.; Duraiswamy, K. N.; Shen, C. K. F.; Tseng, H. R. *Angew. Chem., Int. Ed.* **2011**, *50*, 3084−8.

(4) Stott, S. L.; Hsu, C. H.; Tsukrov, D. I.; Yu, M.; Miyamoto, D. T.; Waltman, B. A.; Rothenberg, S. M.; Shah, A. M.; Smas, M. E.; Korir, G. K.; Floyd, F. P.; Gilman, A. J.; Lord, J. B.; Winokur, D.; Springer, S.; Irimia, D.; Nagrath, S.; Sequist, L. V.; Lee, R. J.; Isselbacher, K. J.; Maheswaran, S.; Haber, D. A.; Toner, M. *Proc. Natl. Acad. Sci. U.S.A.* **2010**, *107*, 18392−7.

(5) Carbonaro, A.; Mohanty, S. K.; Huang, H.; Godley, L. A.; Sohn., L. L. *Lab Chip* **2008**, *8*, 1478−85.

(6) Cheng, X.; Irimia, D.; Dixon, M.; Sekine, K.; Demirci, U.; Zamir, L.; Tompkins, R. G.; Rodriguez, W.; Toner, M. *Lab Chip* **2007**, *7*, 170−8.

(7) Kotz, K. T.; Xiao, W.; Miller-Graziano, C.; Qian, W. J.; Russom, A.; Warner, E. A.; Moldawer, L. L.; De, A.; Bankey, P. E.; Petritis, B. O.; Camp, D. G., II; Rosenbach, A. E.; Goverman, J.; Fagan, S. P.; Brownstein, B. H.; Irimia, D.; Xu, W.; Wilhelmy, J.; Mindrinos, M. N.; Smith, R. D.; Davis, R. W.; Tompkins, R. G.; Toner, M. *Nat. Med.* **2010**, *16*, 1042−7.

(8) Dharmasiri, U.; Witek, M. A.; Adams, A. A.; Soper, S. A. *Annu. Rev. Anal. Chem.* **2010**, *3*, 409−31.

(9) Maheswaran, S.; Sequist, L. V.; Nagrath, S.; Ulkus, L.; Brannigan, B.; Collura, C. V.; Inserra, E.; Diederichs, S.; Iafrate, A. J.; Bell, D. W.; Digumarthy, S.; Muzikansky, A.; Irimia, D.; Settleman, J.; Tompkins, R. G.; Lynch, T. J.; Toner, M.; Haber, D. A. *N. Engl. J. Med.* **2008**, *359*, 366−77.

(10) Wang, K.; Marshall, M.; Garza, G.; Pappas, D. *Anal. Chem.* **2008**, *80*, 2118−2124.

(11) Pappas, D.; Wang, K. *Anal. Chim. Acta* **2007**, *601*, 26−35.

(12) Wang, H.; Riha, G. M.; Yan, S.; Li, M.; Chai, H.; Yang, H.; Yao, Q.; Chen., C. *Arterioscler., Thromb., Vasc. Biol.* **2005**, *25*, 1817.

(13) Adams, A. A.; Okagbare, P. I.; Feng, J.; Hupert, M. L.; Patterson, D.; Göttert, J.; McCarley, R. L.; Nikitopoulos, D.; Murphy, M. C.; Soper, S. A. *J. Am. Chem. Soc.* **2008**, *130*, 8633−8641.

(14) Dharmasiri, U.; Balamurugan, S.; Adams, A. A.; Okagbare, P. I.; Obubuafo, A.; Soper, S. A. *Electrophoresis* **2009**, *30*, 3289−300.

(15) Panchision, D. M.; Chen, H. L.; Pistollato, F.; Papini, D.; Ni, H. T.; Hawley, T. S. *Stem Cells* **2007**, *25*, 1560−70.

(16) Cooperstein, M. A.; Canavan, H. E. *Langmuir* **2010**, *26*, 7695−707.

(17) Kloxin, A. M.; Kasko, A. M.; Salinas, C. N.; Anseth, K. S. *Science* **2009**, *324*, 59−63.

(18) Hatch, A.; Hansmann, G.; Murthy, S. K. *Langmuir* **2011**, *27*, 4257−64.

(19) Gordan, H. G.; Larson, N. L. *Am. J. Clin. Pathol.* **1955**, *23*, 613−18.

(20) International Council for Standardization in Haematology.. *Am. J. Clin. Pathol.* **1993**, *100*, 371−72.

(21) Lewis, S. M.; Stoddart, C. T. *Lab Pract.* **1971**, *10*, 787−92.

(22) Berridge, M. J. In *New Comprehensive Biochemistry*; Krebs, J., Michalak, M., Eds.; Elsevier: 2007; Vol. *41*, pp 485−502.

(23) Machaca, K. *Cell Calcium* **2010**, *48*, 243−50.

(24) Augst, A. D.; Kong, H. J.; Mooney, D. J. *Macromol. Biosci.* **2006**, *6*, 623−33.

(25) Ashton, R. S.; Banerjee, A.; Punyani, S.; Schaffer, D. V.; Kane, R. S. *Biomaterials* **2007**, *28*, 5518−25.
(26) Breguet, V.; von Stockar, U.; Marison, I. W. *Biotechnol. Prog.* **2007**, *23*, 1223−30.
(27) Xia, Y.; Whitesides, G. M. *Annu. Rev. Mater. Sci.* **1998**, *28*, 153−84.
(28) Comisar, W. A.; Kazmers, N. H.; Mooney, D. J.; Linderman, J. J. *Biomaterials* **2007**, *30*, 4409−17.
(29) Comisar, W. A.; Hsiong, S. X.; Kong, H. J.; Mooney, D. J.; Linderman, J. J. *Biomaterials* **2006**, *27*, 2322−9.
(30) Cristofanilli, M.; Budd, G. T.; Ellis, M. J.; Stopeck, A.; Matera, J.; Miller, M. C.; Reuben, J. M.; Doyle, G. V.; Allard, W. J.; Terstappen, L. W. M. M.; Hayes, D. F. *N. Engl. J. Med.* **2004**, *8*, 781−91.
(31) Danila, D. C.; Heller, G.; Gignac, G. A.; Gonzalez-Espinoza, R.; Anand, A.; Tanaka, E.; Lilja, H.; Schwartz, L.; Larson, S.; Fleisher, M.; Scher, H. I. *Clin. Cancer Res.* **2007**, *23*, 7053−8.
(32) Yu, M.; Stott, S.; Toner, M.; Maheswaran, S.; Haber, D. A. *J. Cell Biol.* **2011**, *3*, 373−82.
(33) Jeon, O.; Bouhadir, K.; Mansour, J. M.; Alsberg, E. *Biomaterials* **2009**, *30*, 2724−34.
(34) Haraguchi, K.; Li, H.-J. *Angew. Chem., Int. Ed.* **2005**, *30*, 2724−2734.
(35) Nayak, S.; Lyon, L. A. *Angew. Chem., Int. Ed.* **2005**, *44*, 7686−7708.

Science Translational Medicine
AAAS

Inertial Focusing for Tumor Antigen–Dependent and –Independent Sorting of Rare Circulating Tumor Cells

Emre Ozkumur *et al.*

Sci Transl Med **5**, 179ra47 (2013);
DOI: 10.1126/scitranslmed.3005616

Editor's Summary

Positive and Negative Outcomes

Usually people want the good news first, to help cope with the bad news that inevitably follows. However, patients will soon desire both the positive and the negative outcomes together, according to the latest study by Ozkumur and colleagues. These authors have developed a multistage microfluidic device that is capable of sorting rare circulating tumor cells (CTCs) that are either positive or negative for the surface antigen epithelial cell adhesion molecule (EpCAM).

$EpCAM^+$ cells found in the bloodstream have long defined the typical CTC. Many sorting technologies have been developed to enumerate $EpCAM^+$ CTCs in cancer patient's blood; however, these cells are not always detectable in cancers with low EpCAM expression, like triple-negative breast cancer or melanoma. Ozkumur *et al.* engineered an automated platform, called the "CTC-iChip," that captured both $EpCAM^+$ and $EpCAM^-$ cancer cells in clinical samples using a series of debulking, inertial focusing, and magnetic separation steps. The sorted CTCs could then be interrogated using standard clinical protocols, such as immunocytochemistry. The authors tested the "positive mode" of their device using whole blood from patients with prostate, lung, breast, pancreatic, and colorectal cancers. After successfully separating out the $EpCAM^+$ CTCs, they confirmed that the cells were viable and had high-quality RNA for molecular analysis, in one example, detecting the *EML4-ALK* gene fusion in lung cancer. Using the "negative mode" of their device, the authors were able to capture $EpCAM^-$ CTCs from patients with metastatic breast cancer, pancreatic cancer, and melanoma. The isolated CTCs showed similar morphology when compared with primary tumor tissue from these patients, suggesting that the microfluidic device can be used for clinical diagnoses––delivering both positive and negative news at once.

Ozkumur *et al.* also demonstrated that CTCs isolated using the iChip could be analyzed on the single-cell level. One such demonstration with 15 CTCs from a prostate cancer patient reveals marked heterogeneity in the expression of mesenchymal and stem cell markers as well as typical prostate cancer –related antigens. The CTC-iChip can therefore process large volumes of patient blood to obtain not just $EpCAM^+$ CTCs but also the $EpCAM^-$ ones, thus giving a broader picture of an individual's cancer status and also allowing the device to be used for more cancer types. With the ability to further analyze the molecular characteristics of CTCs, this CTC-iChip could be a promising addition to current diagnostic tools used in the clinic.

Science Translational Medicine (print ISSN 1946-6234; online ISSN 1946-6242) is published weekly, except the last week in December, by the American Association for the Advancement of Science, 1200 New York Avenue NW, Washington, DC 20005.

Science Translational Medicine (print ISSN 1946-6234; online ISSN 1946-6242) is published weekly, except the last week in December, by the American Association for the Advancement of Science, 1200 New York Avenue NW, Washington, DC 20005.

CANCER DIAGNOSTICS

Inertial Focusing for Tumor Antigen–Dependent and –Independent Sorting of Rare Circulating Tumor Cells

Emre Ozkumur,[1]* Ajay M. Shah,[1]* Jordan C. Ciciliano,[2] Benjamin L. Emmink,[1] David T. Miyamoto,[2,3] Elena Brachtel,[4] Min Yu,[2,5] Pin-i Chen,[1] Bailey Morgan,[1] Julie Trautwein,[2] Anya Kimura,[2] Sudarshana Sengupta,[2] Shannon L. Stott,[1,2] Nezihi Murat Karabacak,[1] Thomas A. Barber,[1] John R. Walsh,[1] Kyle Smith,[1] Philipp S. Spuhler,[1] James P. Sullivan,[2,6] Richard J. Lee,[2,6] David T. Ting,[2,6] Xi Luo,[2,5] Alice T. Shaw,[2,6] Aditya Bardia,[2,6] Lecia V. Sequist,[2,6] David N. Louis,[4] Shyamala Maheswaran,[2,7] Ravi Kapur,[1] Daniel A. Haber,[2,5,6] Mehmet Toner[1,7†]

Circulating tumor cells (CTCs) are shed into the bloodstream from primary and metastatic tumor deposits. Their isolation and analysis hold great promise for the early detection of invasive cancer and the management of advanced disease, but technological hurdles have limited their broad clinical utility. We describe an inertial focusing–enhanced microfluidic CTC capture platform, termed "CTC-iChip," that is capable of sorting rare CTCs from whole blood at 10^7 cells/s. Most importantly, the iChip is capable of isolating CTCs using strategies that are either dependent or independent of tumor membrane epitopes, and thus applicable to virtually all cancers. We specifically demonstrate the use of the iChip in an expanded set of both epithelial and nonepithelial cancers including lung, prostate, pancreas, breast, and melanoma. The sorting of CTCs as unfixed cells in solution allows for the application of high-quality clinically standardized morphological and immunohistochemical analyses, as well as RNA-based single-cell molecular characterization. The combination of an unbiased, broadly applicable, high-throughput, and automatable rare cell sorting technology with generally accepted molecular assays and cytology standards will enable the integration of CTC-based diagnostics into the clinical management of cancer.

INTRODUCTION

The rarity of circulating tumor cells (CTCs) in the blood of cancer patients has required development of highly specialized technologies for their isolation (*1, 2*). Once detected, enumeration and molecular characterization of CTCs have been applied to prognostic classifications of breast, prostate, and colon cancers (*3*), and to predictive markers of targeted drug therapy in lung cancer (*4*). However, the limited sensitivity of commercially available approaches combined with the complexity and heterogeneity of the disease has restricted the broad acceptance and dissemination of CTC-based diagnostics (*5*).

Several strategies have been used to process blood for analysis of CTCs, including platforms for rapid scanning of unpurified cell populations (*6–8*). The most common enrichment approaches have used antibodies against the cell surface protein epithelial cell adhesion molecule (EpCAM). Labeling CTCs with anti-EpCAM–coated beads, followed by bulk magnetic enrichment methods (*9–11*), has been tested. The U.S. Food and Drug Administration (FDA)–approved Veridex system, CellSearch, immunomagnetically labels CTCs and then enriches the cells by bulk purification across a magnetic field. Conceptually, EpCAM-based CTC capture may have limited ability to identify tumor cells with reduced expression of this epithelial marker as a result of the epithelial-mesenchymal transition (EMT) (*12*). However, tumor antigen–independent CTC enrichment, such as bulk depletion of hematopoietic cells, suffers from poor yields and low purity (*13, 14*). Together, CTC isolation approaches have traditionally involved multiple batch processing steps, resulting in substantial loss of CTCs (*14*).

Recently, we introduced microfluidic methods to improve the sensitivity of CTC isolation (*15*), a strategy that is particularly attractive because it can lead to efficient purification of viable CTCs from unprocessed whole blood (*16–21*). The micropost CTC-Chip ($^{\mu P}$CTC-Chip) relies on laminar flow of blood cells through anti-EpCAM antibody-coated microposts (*15*), whereas the herringbone CTC-Chip (^{Hb}CTC-Chip) uses microvortices generated by herringbone-shaped grooves to direct cells toward antibody-coated surfaces (*16*). Although promising, these methods require surface functionalization to bind to tumor antigens on CTCs and thus yield CTCs that are immobilized within a microfluidic chamber and are not readily subjected to either standard clinical cytopathological imaging or single-cell molecular characterization.

To address the shortcomings of the current approaches, we developed a strategy that combines the strengths of microfluidics for rare cell handling while incorporating the benefits of magnetic-based cell sorting. After the magnetic labeling of cells in whole blood, this capture platform integrates three sequential microfluidic technologies within a single automated system: (i) debulking by separation of nucleated cells, including CTCs and white blood cells (WBCs), from red blood cells (RBCs) and platelets using deterministic lateral displacement (*22*); (ii) alignment of nucleated cells within a microfluidic channel using inertial focusing (*23*); and (iii) deflection of magnetically tagged cells into a collection

[1]Massachusetts General Hospital Center for Engineering in Medicine, Harvard Medical School, Boston, MA 02114, USA. [2]Massachusetts General Hospital Cancer Center, Harvard Medical School, Boston, MA 02114, USA. [3]Department of Radiation Oncology, Massachusetts General Hospital, Harvard Medical School, Boston, MA 02114, USA. [4]Department of Pathology, Massachusetts General Hospital, Harvard Medical School, Boston, MA 02114, USA. [5]Howard Hughes Medical Institute, Chevy Chase, MD 20815, USA. [6]Department of Medicine, Massachusetts General Hospital, Harvard Medical School, Boston, MA 02114, USA. [7]Department of Surgery, Massachusetts General Hospital, Harvard Medical School, Boston, MA 02114, USA.
*These authors contributed equally to this work.
†Corresponding author. E-mail: mtoner@hms.harvard.edu

channel. In essence, these three integrated microfluidic functions replace bulk RBC lysis and/or centrifugation, hydrodynamic sheath flow in flow cytometry, and magnetic-activated cell sorting (MACS). We call this integrated microfluidic system the CTC-iChip, based on the inertial focusing strategy, which allows positioning of cells in a near-single file line, such that they can be precisely deflected using minimal magnetic force. This integrated microfluidic platform, with its ability to isolate CTCs in suspension using both tumor antigen–dependent and tumor antigen–independent modes, is compatible with high-definition imaging and single-cell molecular analyses, as well as standard clinical cytopathology. We demonstrate its capabilities for diverse cancer diagnostic applications in both epithelial and nonepithelial cancers.

RESULTS

CTC-iChip design and function

The overall CTC-iChip isolation strategy is depicted in Fig. 1 and fig. S1. We explored two modes of immunomagnetic sorting to isolate CTCs: a positive selection mode (^{pos}CTC-iChip), whereby CTCs are identified and sorted on the basis of their expression of EpCAM, and a negative selection mode (^{neg}CTC-iChip), in which the blood sample is depleted of leukocytes by immunomagnetically targeting both the common leukocyte antigen CD45 and the granulocyte marker CD15.

Target cell labeling was developed and characterized for both operational modes (fig. S2). After labeling, the first stage within the CTC-iChip used hydrodynamic size–based sorting to achieve low shear microfluidic debulking of whole blood (*22*, *24*). RBCs, platelets, plasma proteins, and free magnetic beads were discarded, whereas nucleated cells (WBCs and CTCs) were retained and presented to the second stage for inertial focusing. The efficient removal of free beads is critical because these may accumulate in the magnetophoresis channel and significantly reduce the sensitivity and specificity of the approach. The operational principle of microfluidic debulking is based on hydrodynamic size–dependent deterministic lateral displacement (*22*, *24*), in which coincident flow of cell-containing and cell-free solutions through an array of microposts leads to rapid size-based separation (Fig. 1C and fig. S3). We tested two different array configurations with gaps between

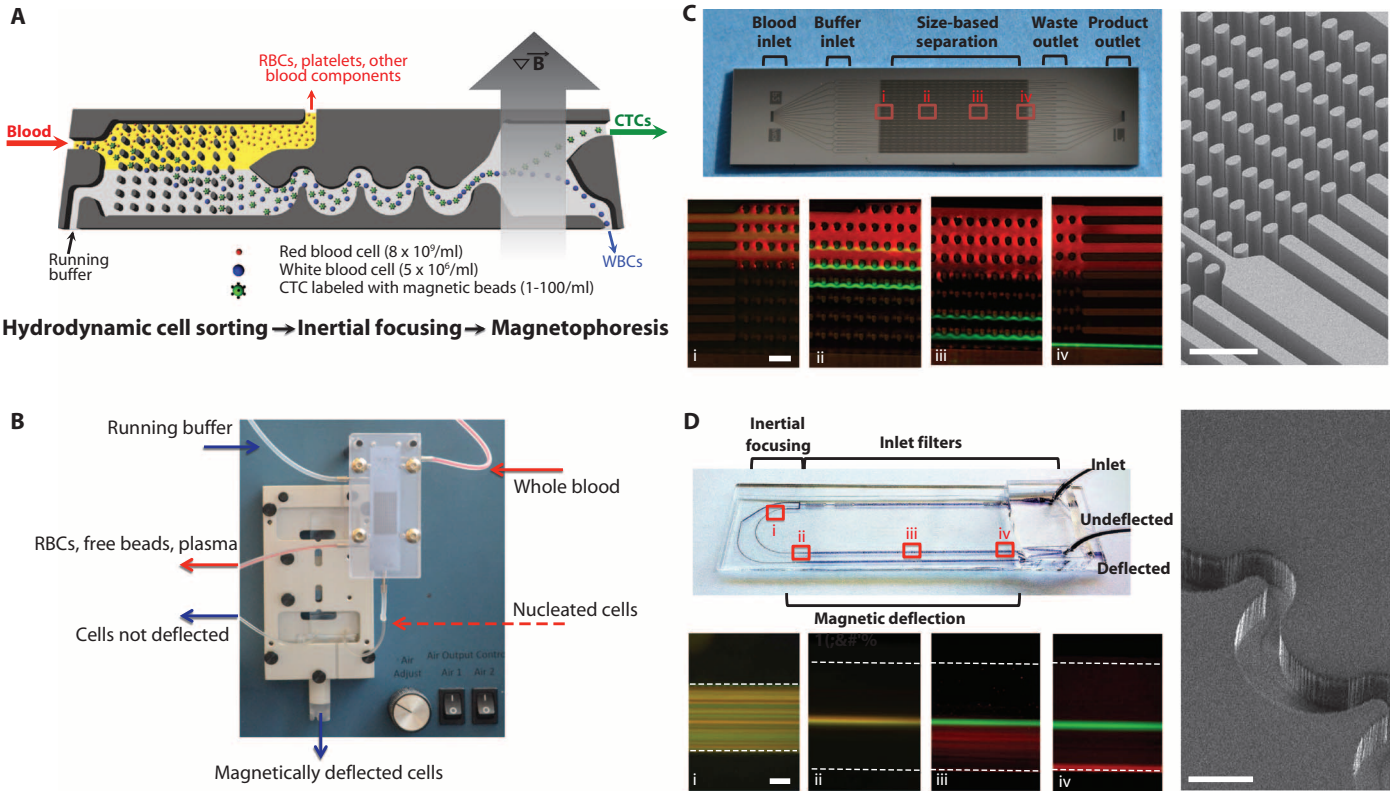

Fig. 1. The CTC-iChip system. (**A**) Three microfluidic components of the CTC-iChip are shown schematically. Whole blood premixed with immunomagnetic beads and buffer comprises the inputs. The figure demonstrates the positive isolation method; however, the system can be operated in negative depletion mode. (**B**) Integrated microfluidic system. The debulking array sits in a custom polycarbonate manifold that enables fluidic connections to the inputs, waste line, and second-stage microfluidic channels. The inertial focusing and magnetophoresis chip is placed in an aluminum manifold that houses the quadrupole magnetic circuit. Magnetically deflected cells are collected in a vial. (**C**) Hydrodynamic size–based sorting. A mixture of 2-μm (red) and 10-μm (green) beads enters the channel (i). Whereas the 2-μm beads remain in laminar flow and follow the fluid streamlines, the 10-μm spheres interact with the post-array (ii and iii) as shown in the scanning electron microscope (SEM) image (right panel). Larger beads are fully deflected into the coincident running buffer stream by the end of the array (iv). Scale bars, 100 μm. (**D**) Cell focusing and magnetophoretic sorting. Magnetically labeled SKBR3 (red) and unlabeled PC3-9 (green) cell populations are mixed and enter the channel in random distribution (i). After passing through 60 asymmetric focusing units (pictured in the SEM, right panel), the cells align in a single central stream (ii). Magnetically tagged cells are then deflected (iii) using an external magnetic field, and separation is achieved by the end of the channel (iv). Scale bars, 100 μm.

microposts of 20 or 32 μm. An array with 20-μm gaps retains virtually all nucleated cells with minimal contaminating RBCs but has a cutoff for cells larger than 21 μm and may therefore lose large CTCs or CTC clusters. In contrast, an array with 32-μm gaps has an extended operating range for cells between 8 and 30 μm but retains only 60% of WBCs. Because the cells lost in the 32-μm gap array are granulocytes and lymphocytes that are smaller than the reported CTC sizes (*16*), we selected this array for the CTC-iChip.

The second CTC-iChip component orders nucleated cells within the microfluidic channel, both laterally and longitudinally, so they can be precisely deflected into a collection channel with minimal magnetic moment. The rationale underlying the inertial focusing of cells in microchannels is based on the principles of pipe flow (*23*, *25*); essentially, a cellular fluid entering asymmetric, curved channels emerges as a tight row of individual cells traveling within a defined streamline position (Fig. 1D). We tested variable cell suspensions for focusing performance; WBCs as well as cancer cell lines were well focused within the operational parameters (hematocrit less than 0.4%; flow rate between 50 and 150 μl/min; nucleated cell concentration less than 3×10^6/ml) (fig. S4). Inertial focusing operational parameters were matched to output of the preceding debulking array, and the in-line integration of these complex microfluidic structures within the CTC-iChip thus avoided cell losses associated with commonly used batch processing strategies.

In the final CTC-iChip component, magnetically labeled cells are separated from unlabeled cells within a deflection channel. The precise control over cell position provided by inertial focusing prevents cellular collisions during magnetophoresis; therefore, cell displacement occurs as a predictable function of magnetic load. We modeled the forces exerted on cells labeled with 1-μm beads using a quadrupole magnetic circuit (fig. S5) and predicted deflection patterns under different flow and magnetic load conditions (Fig. 2A). This model was tested using magnetically labeled PC3-9 human prostate cancer cells. The measured deflection distance, plotted as a function of magnetic load, matched the prediction (Fig. 2B).

To demonstrate the dependence of sensitivity on flow speed, we processed labeled cells at various flow rates and quantified the number of beads per cell for deflected and nondeflected outputs (Fig. 2C and fig. S6). The improvement in sensitivity with increasing magnetic residence time (by reducing flow speed) correlated with the predictive model (Fig. 2D), indicating high magnetic sensitivity for the overall system (5 to 20 beads per cell, depending on cell size). The process parameters characterized for the ^{pos}CTC-iChip applied similarly to the ^{neg}CTC-iChip.

Evaluating the CTC-iChip using cells spiked into whole blood

To evaluate the efficiency of the CTC-iChip, we spiked five cell lines spanning a broad range of EpCAM expression into healthy whole blood and isolated using ^{pos}CTC-iChip or ^{neg}CTC-iChip modes. The EpCAM expression of each cell line was quantified by comparing the anti-EpCAM signal to that of a matched irrelevant antibody (Fig. 3A). Recovery of SKBR3 human breast cancer cells [24-fold EpCAM signal over control immunoglobulin G (IgG)] was 98.6 ± 4.3% (mean ± SD), and capture of human prostate PC3-9 cancer cells (3.7-fold EpCAM signal) was 89.7 ± 4.5% (Fig. 3B). Even cells with minimal EpCAM expression, such as MDA-MB-231 (*26*), a "triple-negative" mesenchymal breast

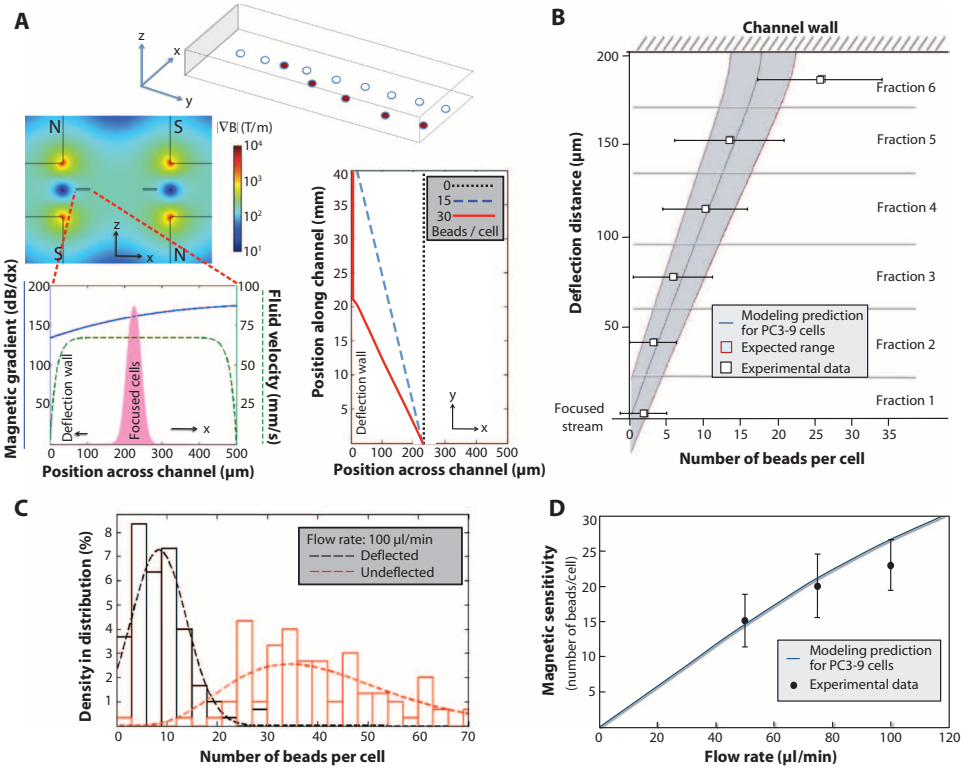

Fig. 2. Modeling and magnetic sensitivity of the system. (**A**) A mathematical model describes the deflection of labeled cells (red) from a focused stream (white). Finite element method analysis of the quadrupole magnetic circuit and fluid flow in the channel provided estimates of the magnetic gradient (blue) and flow rate (green) across the deflection channel (left panel). This information, in conjunction with our experimental understanding of cell position in the focused stream (pink), was used to construct an overall model to predict the trajectories of focused cells with varying magnetic loads (right panel). (**B**) High sensitivity of inertial focusing enhanced magnetophoresis. Human PC3-9 cells were labeled with varying numbers of magnetic beads and collected in separate exit streams after traveling in the 4-cm-long magnetic deflection channel, fractionating the cells based on magnetic deflection distance. The beads on a representative population of cells were counted in each fraction. The deflection distance was measured from focused stream position to the channel wall. Fraction 6 included cells that deflected all the way and traveled at the wall; therefore, this data point did not match the simulation. The expected variations in cell sizes and the initial distribution of cells in the focused stream contribute to a variation in the deflection pattern that is reflected by shading the expected range around the model prediction. (**C**) The experimental "magnetic sensitivity" was determined by plotting histograms of bead loading density for deflected and undeflected cells for a given flow rate. The intersection of curve fits of these data represents the minimum number of beads required to deflect a cell. (**D**) The minimum required magnetic load increases with higher flow rates, as expected, and is accurately predicted by the model.

cancer cell line (only 2.5-fold EpCAM signal over control), were recovered with 77.8 ± 7.8% capture efficiency by ^{pos}CTC-iChip. Virtually complete abrogation of EpCAM expression, achieved by ectopic expression of the EMT master regulator LBX1 in MCF10A human breast cancer cells (MCF10A-LBX1) (*27*), resulted in 10.9 ± 3.0% capture efficiency.

Switching to the ^{neg}CTC-iChip, both the epithelial parental MCF10A cells and their highly mesenchymal MCF10A-LBX1 derivatives were captured at equal efficiency (96.7 ± 1.9% for MCF10As and 97.0 ± 1.7% for the MCF10A-LBX1 derivatives) (Fig. 3B). Together, these two modes demonstrate the flexibility of the CTC-iChip to isolate a broad spectrum of rare cells with high efficiency in both tumor antigen–dependent and tumor antigen–independent modes.

Sample purity was analyzed for both operating modes. Using EpCAM-based positive selection, we achieved an average >3.5-log purification (mean, 1500 WBCs/ml of whole blood; range, 67 to 2537 WBCs/ml). In the leukocyte depletion mode, purification was 2.5 log (mean, 32,000 WBCs/ml; range, 17,264 to 39,172 WBCs/ml) (Fig. 3C). In the ^{pos}CTC-iChip, the vast majority of contaminating WBCs carried magnetic beads, suggesting that nonspecific interactions between WBCs and either the anti-EpCAM antibody or the beads themselves caused the contamination. In the ^{neg}CTC-iChip, contaminating WBCs were free of beads, suggesting that they comprise a population of leukocytes with reduced CD45 or CD15 expression, as confirmed by flow cytometry (table S1).

^{pos}CTC-iChip isolation of CTCs

We tested the ^{pos}CTC-iChip in patients with prostate cancer, a disease in which metastatic lesions primarily affect bone, and hence, CTC analysis is key to analyzing recurrences after resection of the primary tumor. On average, 10 ml (range, 6 to 12 ml) of whole blood was analyzed from these patients. Using triple staining for cytokeratins (CKs) (epithelial marker), CD45 (leukocytes), and 4′,6-diamidino-2-phenylindole (DAPI) (nuclear marker), we identified ≥0.5 CTC/ml in 37 of 41 (90%) prostate patients with recurrent (castration-resistant) disease (mean, 50.3/ml; range, 0.5 to 610/ml; median, 3.2/ml) (Fig. 4A). The detection cutoff of 0.5 CTC/ml was more than 2 SDs above the mean number of CK$^+$ cells detected in 13 healthy donors (excluding an outlier with 0.7/ml; mean ± SD, 0.17 ± 0.12/ml; median, 0.19/ml; range, 0 to 0.33/ml). WBC contamination in the ^{pos}CTC-iChip product was low (mean, 1188/ml; median, 352/ml; range, 58 to 9249/ml), resulting in high sample purities (mean, 7.8%; median, 0.8%; range for samples with ≥0.5 CTC/ml, 0.02 to 43%) (fig. S7).

We performed a detailed comparison of the ^{pos}CTC-iChip with the FDA-approved CellSearch system (Fig. 4B). To minimize reagent variability between platforms, we used anti-EpCAM capture as well as CK and CD45 staining antibodies from the same source, and consistent criteria were used to evaluate putative CTCs. CTCs were defined as DAPI$^+$/CD45$^-$/CK$^+$, and WBCs were defined as DAPI$^+$ or DAPI$^+$/CD45$^+$ events. Specimens from prostate (n = 19) and other cancers (breast, n = 12; pancreas, n = 6; colorectal, n = 2; lung, n = 2) were compared. Although both assays performed well with high CTC loads (>30 CTCs per 7.5 ml), at lower CTC numbers, there was a marked differential in capture efficiency. Among the 86% (36 of 42) of metastatic cancer patients with fewer than 30 CTCs/7.5 ml, the number of CK$^+$ CTCs isolated with the ^{pos}CTC-iChip was significantly higher in 22 cases (P < 0.001, paired t test analysis). The remaining 14 cases had CTCs below detection limits for both systems (Fig. 4B and table S2). Thus, the sensitivity of the CTC-iChip is particularly critical in patients with a lower CTC burden.

In addition to capturing more CTCs in patients with lower CTC burdens, the iChip isolates these cells in suspension, which in turn enables their immobilization on a standard glass slide for high-resolution imaging and standard clinical cytopathological examination (fig. S8), as well as simultaneous staining for multiple biomarkers (Fig. 4, C and D). Beyond imaging, molecular genetic tools are increasingly applied to the characterization of CTCs. Nowhere is this more evident than in non–small cell lung cancer (NSCLC), where targeted therapies can provide marked clinical benefit (*28*). Among the most challenging assays is detection of the *EML4-ALK* translocation in about 3% of cases, which marks those responsive to the selective

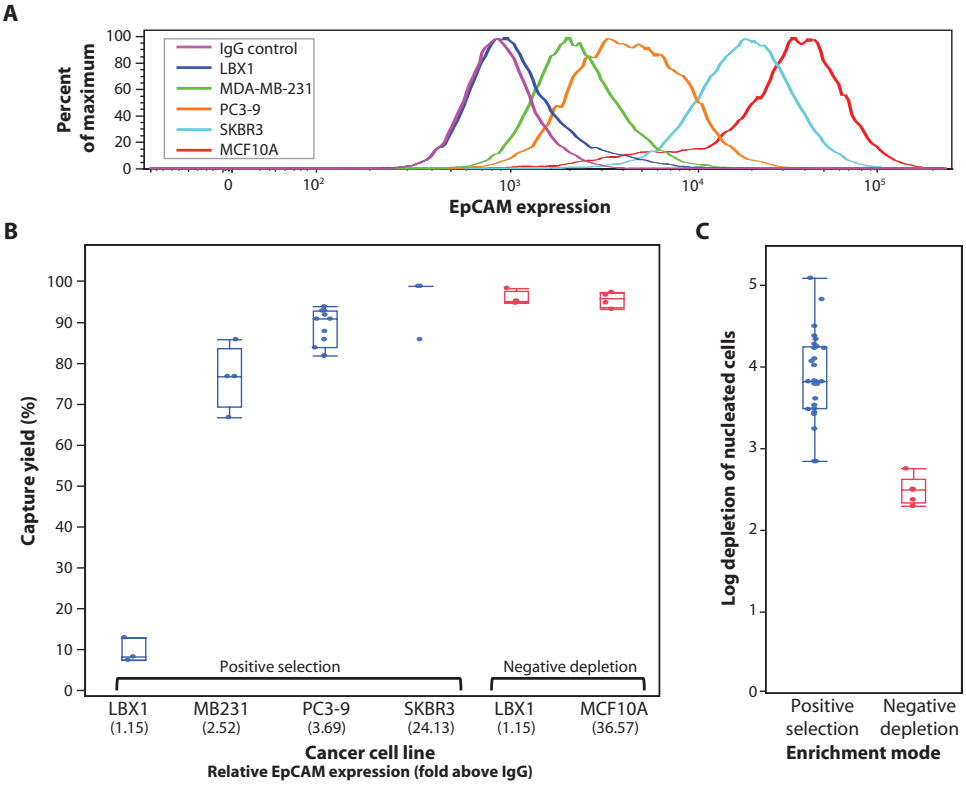

Fig. 3. Evaluation of overall system performance using cancer cell lines spiked into whole blood. (**A**) Quantitation of variable EpCAM expression in five cell lines using flow cytometry. (**B**) Capture yield of positive selection and negative depletion modes using various cell lines expressing different levels of EpCAM. (**C**) Background in ^{pos}CTC-iChip product is measured, achieving >3.5-log depletion of WBCs. In contrast, ^{neg}CTC-iChip has an order of magnitude lower purification. In both (B) and (C), each data point is an experimental result. Upper and lower bounds of the boxes signify the 75th and 25th quantiles, respectively. Perpendicular line in the box represents median value, and data points left above or below the error bars are outliers.

targeted inhibitor crizotinib. Detection of this intrachromosomal translocation by fluorescence in situ hybridization (FISH) is difficult, and, at the molecular level, the variability of chromosomal breakpoints necessitates RNA-based detection of the fusion transcript, which cannot be readily achieved using either fixed CTCs or free plasma nucleic acids.

We established a reverse transcription polymerase chain reaction (RT-PCR) assay capable of detecting the *EML4-ALK* translocation in H3122 lung cancer cells spiked into WBCs at a purity of 0.1% or introduced into whole blood (10 cells/10 ml) and processed through the ^{pos}CTC-iChip (Fig. 4E). In patient specimens, the *EML4-ALK* transcript was detected in CTCs from four cases known to have this chromosome rearrangement by FISH analysis of the primary tumor. It was absent in CTCs from two NSCLC patients and one patient with prostate cancer whose tumors were all known to lack this abnormality. In cases where CTC-based RNA analysis identified the expected product, nucleotide sequencing confirmed the breakpoint in the fusion transcript (Fig. 4F). Thus, the ^{pos}CTC-iChip allowed purification of CTCs for RNA-based molecular genotyping.

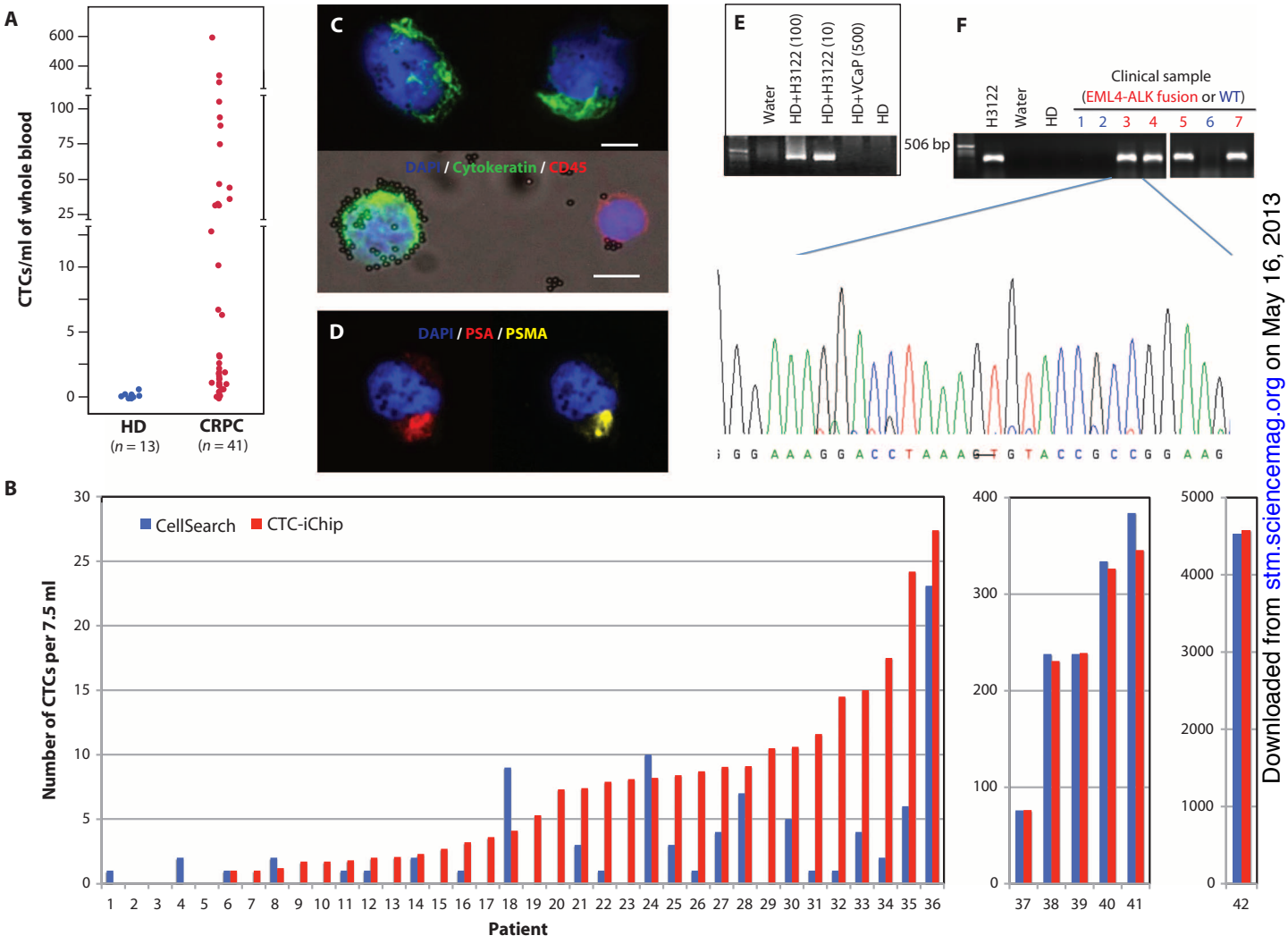

Fig. 4. CTC isolation by ^{pos}CTC-iChip in cancer patients. (**A**) CTCs isolated from castrate-resistant prostate cancer (CRPC) patients were enumerated and compared with blood specimens processed from healthy donors. (**B**) EpCAM-based isolation using ^{pos}CTC-iChip was compared with the CellSearch system. Clinical samples were metastatic cancer patients of prostate (n = 19), breast (n = 12), pancreas (n = 6), colorectal (n = 2), and lung (n = 2). All counts were normalized to 7.5 ml. (**C**) For enumeration of CTCs from CRPC patients, CK8/18/19 staining was used (green). CD45 antigen (red) was used to identify contaminating leukocytes. Scale bars, 10 μm. (**D**) A CTC from a CRPC patient was stained for prostate-specific antigen (PSA) (red), prostate-specific membrane antigen (PSMA) (yellow), and DAPI (blue) to demonstrate dual immunofluorescence staining for PSAs. (**E**) Validation of *EML4-ALK* RT-PCR assay was completed with cell lines. ^{pos}CTC-iChip products of whole blood from a healthy donor (HD) spiked with 0, 10, and 100 H3122 cells (expressing *EML4-ALK* variant 1) per 10 ml were subjected to RT-PCR for detection of the *EML4-ALK* fusion. Product isolated from healthy donor blood spiked with 500 VCaP cells/ml was processed as a negative control. (**F**) ^{pos}CTC-iChip products from patient samples known to harbor the *EML4-ALK* translocation by FISH were similarly processed as in (E), and the bands were sequenced to confirm the presence of the fusion transcript. A representative sequence trace from patient 3 shows the translocation breakpoint between exon 13 of *EML4* and exon 20 of *ALK*. CTC analysis of three patients whose cancer lacks the translocation was used to establish specificity: a prostate cancer patient (lane 1), an *EGFR* mutant lung cancer patient (lane 2), and a *HER2*-amplified lung cancer patient (lane 6).

^{neg}CTC-iChip to isolate CTCs

Given the heterogeneity of circulating cancer cells, including the subset thought to undergo EMT, depletion of normal blood cells from clinical specimens should allow characterization of unlabeled nonhematopoietic cells. We analyzed CTCs from 10 patients with metastatic breast cancer, including luminal (ER^+/PR^+, $n = 6$), triple-negative ($ER^-/PR^-/HER2^-$, $n = 2$), and $HER2^+$ ($n = 2$) subtypes. Triple-negative breast cancers are noteworthy in that they express primarily mesenchymal markers and are unlikely to be captured efficiently using positive selection for $EpCAM^+$ cells (*20*).

We stained the enriched CTC specimens using the Papanicolaou (Pap) stain, which is used for cytopathology analysis in clinical laboratories. In selected cases, the hematoxylin and eosin (H&E)–stained primary tumor tissue was compared with Pap-stained fine needle aspirates (FNAs) of the tumor or pleural effusions from the same patient. A remarkably similar morphological appearance was evident between cancer cells in the primary breast tumors and the isolated CTCs, as shown for three different patients in Fig. 5A. An ER^+ breast cancer patient revealed small and regularly shaped cells in H&E, cytology, and CTC samples. Similarly, larger and more irregular tumor cells were found in a $HER2^+$ primary breast cancer by H&E cytology and CTC analysis. In another example from a triple-negative high-grade breast cancer patient, pleomorphic CTCs similar to the patient's previously sampled cytology specimen were seen.

We extended these morphological analyses to pancreatic cancer and melanoma with similar findings (Fig. 5A). For these, pancreatic adenocarcinoma showed CTCs of comparable size to the primary tumor by both histology and Pap cytology. Conversely, melanoma consisted of dyshesive tumor cells. The spindled cytoplasm in melanoma was also

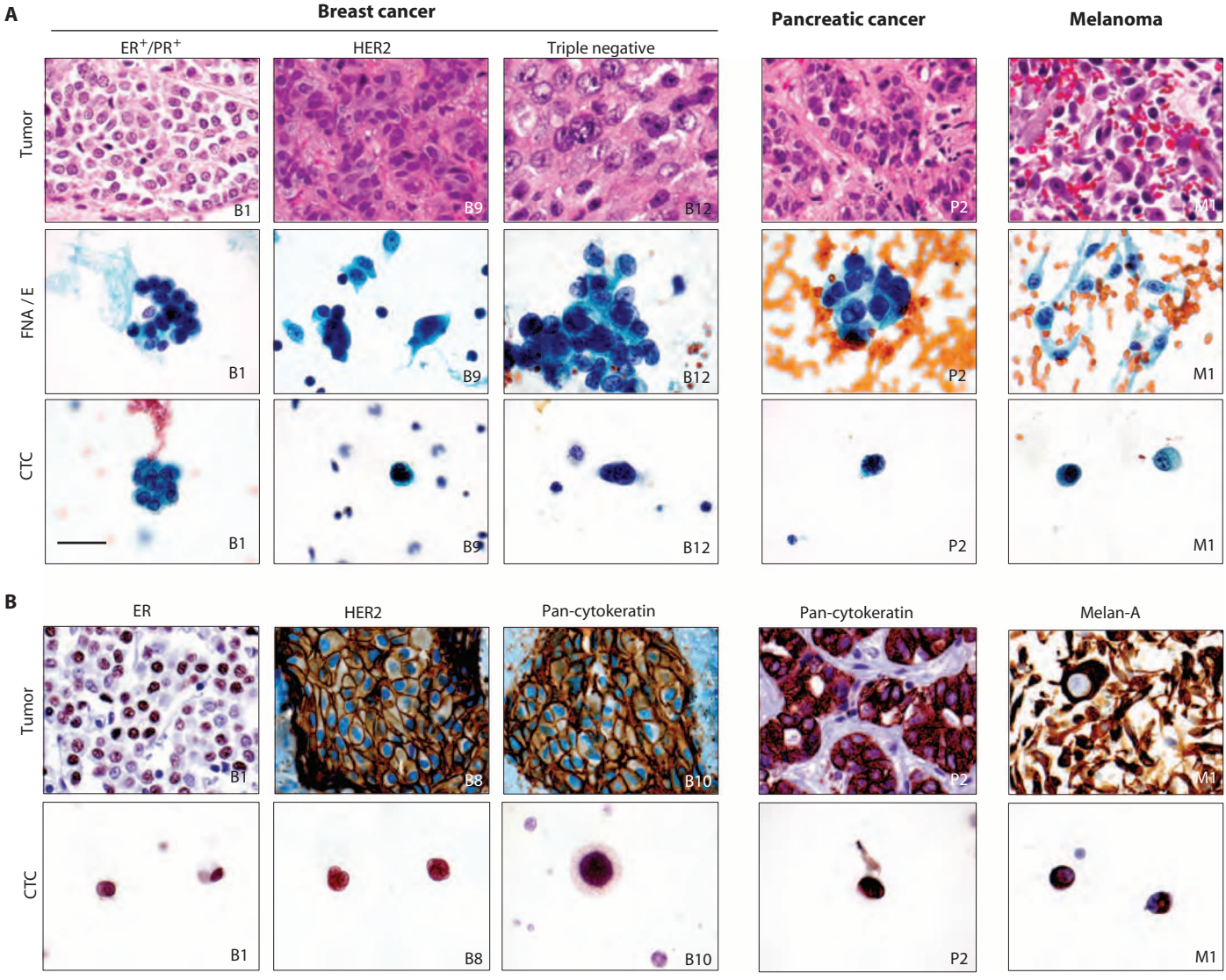

Fig. 5. Classification of CTCs with cytopathology and ICC. (**A**) Specimens from H&E-stained primary and metastatic tumors (upper row) are compared with matched Pap-stained cytology samples from FNAs or pleural effusions (FNA/E) (middle row) and Pap-stained CTCs enriched from blood samples of the same patient using ^{neg}CTC-iChip (lower row). Marked morphological similarity is seen between isolated CTCs and main tumors or cytology samples. (**B**) ICC profiles of primary and metastatic tumors (upper panel) matched to CTCs from the same patient (lower panel). All images: ×1000 original magnification. Scale bar is 30 μm and valid for all images.

seen on the cytology preparation, but the CTCs appeared round. As a neural crest–derived malignancy, melanoma cells do not express EpCAM, and hence, their detection requires the ^{neg}CTC-iChip isolation mode. Nevertheless, on the basis of established cellular and nuclear morphology criteria, our CTC analyses were considered to be of sufficient quality to enable a clinical diagnosis of suspicious for malignancy.

Pap-stained CTC slides were destained and then subjected to immunocytochemistry (ICC), which was first validated through cell lines (fig. S9). ICC of CTCs identified estrogen receptor (ER) protein in luminal breast cancer cells, keratin in triple-negative cells, and strong HER2 staining in cells from HER2$^+$ breast cancers (Fig. 5B and fig. S10). Similarly, CTCs from patients with pancreatic cancer stained positive by ICC for CK, and CTCs from melanoma patients stained positive for the melanocytic marker Melan-A (Fig. 5B and fig. S10). The combination of Pap staining followed by ICC enabled enumeration of CTCs isolated by ^{neg}CTC-iChip despite the presence of surrounding leukocytes.

Not all cytologically suspicious cells (for example, large cells with large, irregular nuclei as identified on the Pap-stained CTC slide) could be confirmed as tumor cells by ICC staining. Conversely, cells that were not scored as CTCs on initial cytological evaluation were subsequently identified as tumor cells by ICC, reflecting substantial heterogeneity in CTC size and morphology (fig. S11). Thus, by not relying exclusively on immunofluorescence-based scoring of CK$^+$ cells, we were able to apply to CTCs the same rigorous morphological and immunohistochemical criteria used by clinical cytopathologists in the diagnosis of malignancy.

We observed large variation in CTC size among different cancer types. Although some CTCs were larger than leukocytes, there was considerable overlap between the two cell populations (Fig. 6). The variation in CTC size was not restricted to different cancer histologies. In one patient with ER$^+$/PR$^+$ breast cancer whose CTCs were isolated using the ^{neg}CTC-iChip and analyzed using a combination of Pap stain and ICC, we identified CTCs ranging from 9 to 19 μm in diameter.

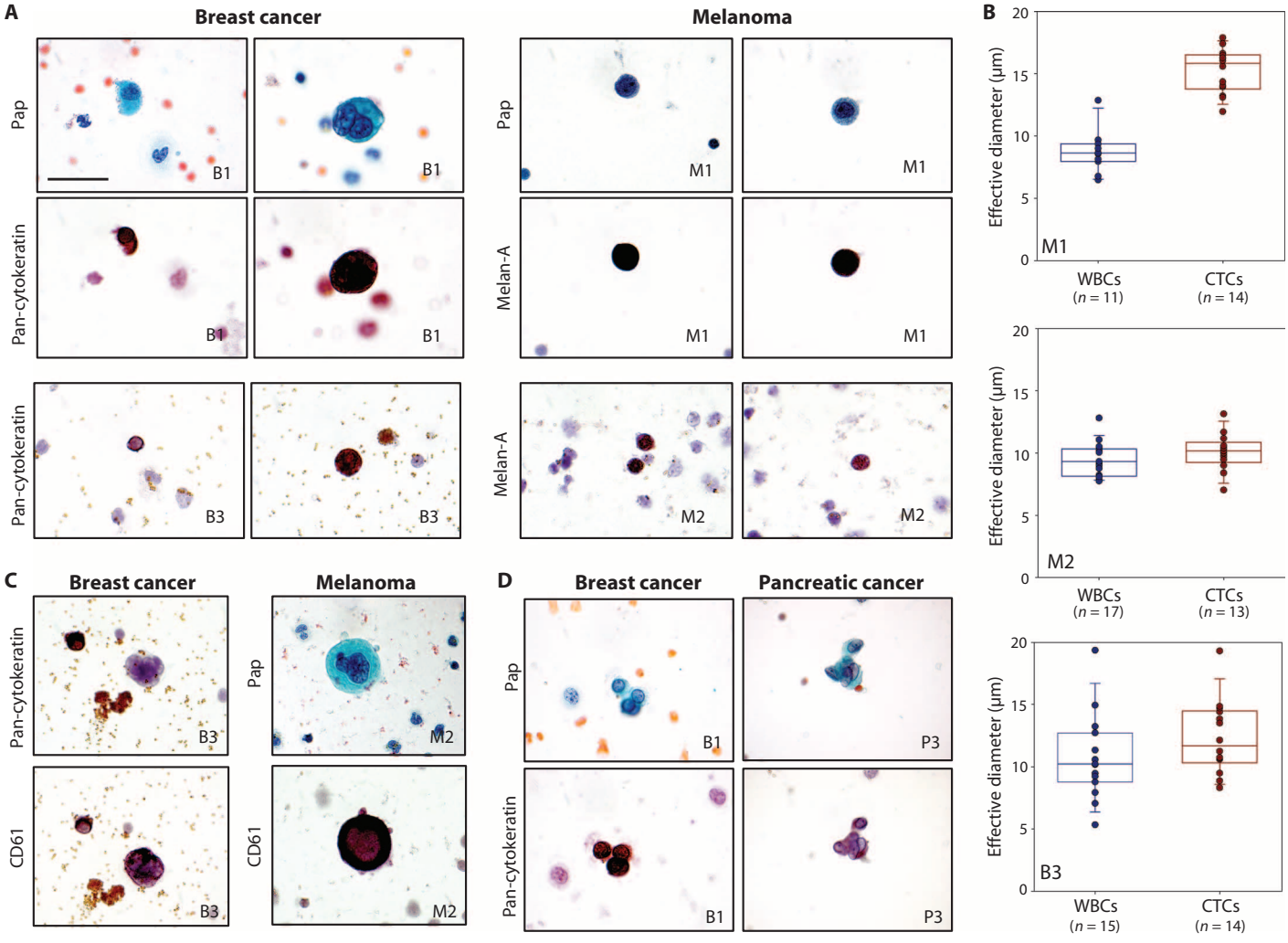

Fig. 6. Variation of CTC sizes and morphologies. (**A**) CTCs from breast cancer and melanoma patients consecutively stained with Pap and either anti-CK (breast) or anti–Melan-A (melanoma) antibodies. (**B**) Quantitative analysis of the effective diameter (maximum feret diameter) for individual cells isolated in three cases. The top two panels are from different melanoma patients (M1 and M2). The bottom panel is from a breast cancer patient (B3). (**C**) Occasional very large cells with ample cytoplasm and multilobed nuclei were initially considered suspicious but were CK$^-$. The same cells were subsequently restained for the platelet marker CD61, which supports their identification as circulating megakaryocytes. (**D**) CTCs were occasionally observed as clusters and confirmed by positive CK staining. All images: ×1000 original magnification. Scale bar, 30 μm.

Although most melanoma CTCs were large in size (>12 μm), one patient with metastatic melanoma had numerous CTCs less than 10 μm in diameter, detected using Pap and ICC for Melan-A (Fig. 6, A and B). In breast cancer and melanoma patients, some very large atypical cells (>30 μm) identified by Pap staining as having multilobed nuclei were at first assumed to be CTCs. However, ICC staining for the platelet marker CD61 confirmed their identity as megakaryocytes (Fig. 6C). Finally, application of the ^{neg}CTC-iChip platform identified clusters of two to six CK$^+$ CTCs in breast and pancreatic cancers, consistent with our previous detection of CTC clusters using the ^{Hb}CTC-Chip (*16*) (Fig. 6D). The negative selection mode of the CTC-iChip thus provided a comprehensive and unbiased view of nonhematological cells in the bloodstream of cancer patients.

Single-cell RNA expression in CTCs

Global CTC expression analyses may identify major pathways involved in metastasis (*20*), but the inherent heterogeneity of CTCs necessitates the identification of expression patterns and signaling pathways within individual cells. We therefore applied a series of single-cell micromanipulation approaches to interrogate individual CTCs isolated from a patient with prostate cancer using the ^{neg}CTC-iChip. Although micromanipulation approaches require expertise and can be time-consuming, the fact that the CTCs are unadulterated allows for more accurate RNA-based expression profiling than isolated fixed cells. EpCAM$^+$ CTCs were distinguished from contaminating CD45$^+$ leukocytes within the ^{neg}CTC-iChip product by immunostaining (Fig. 7, A and B). CTCs identified as EpCAM$^+$/CD45$^-$ were individually isolated and subjected to RNA analysis by multigene microfluidic quantitative RT-PCR (qRT-PCR), profiling for a panel of transcripts implicated in androgen receptor (AR) signaling, cellular proliferation, stem cell, epithelial and mesenchymal cell fates, and leukocyte-specific lineage (Fig. 7C). Single cells from the human prostate cancer cell line LNCaP were used to optimize assay conditions (fig. S12).

A marked heterogeneity was apparent among 15 CTCs isolated from a single patient with metastatic CRPC who had progressed through multiple lines of therapy, including androgen deprivation therapy with leuprolide, the chemotherapeutic drug docetaxel, and the second-line androgen biosynthesis inhibitor abiraterone acetate. Consistent with EpCAM$^+$ immunostaining, 13 of the 15 CTCs were positive for epithelial gene expression, of which 2 CTCs were dual positive for epithelial as well as mesenchymal markers vimentin and N-cadherin (Fig. 7D). Thus, a subset of CTCs appears to have undergone partial EMT. CTC heterogeneity was also evident with expression of stem cell markers [Nanog, Oct-4 (POU5F1), and c-Myc] in 10 of the 15 CTCs, which overlapped primarily with epithelial markers within individual CTCs (Fig. 7C). Proliferation markers cyclin B, cyclin D, Aurora A kinase, and MYBL2 were detected in another subset of seven CTCs.

AR activity, previously defined in CTCs as the ratio of androgen-driven PSA to androgen-repressed PSMA expression (*21*), was heterogeneous among CTCs. The "AR on" phenotype (PSA expression only) was only seen in 2 of the 15 CTCs, whereas the "AR-off" state (PSMA only) was evident in 2 CTCs, and the "mixed AR" state (PSA$^+$/PSMA$^+$) in 10 CTCs (Fig. 7D). This distribution is concordant with single-cell immunofluorescence analysis of AR signaling status in CTCs from patients with CRPC (*21*).

DISCUSSION

The CTC-iChip described here has the ability to process large volumes of whole blood (8 ml/hour), with high throughput (10^7 cells/s) and

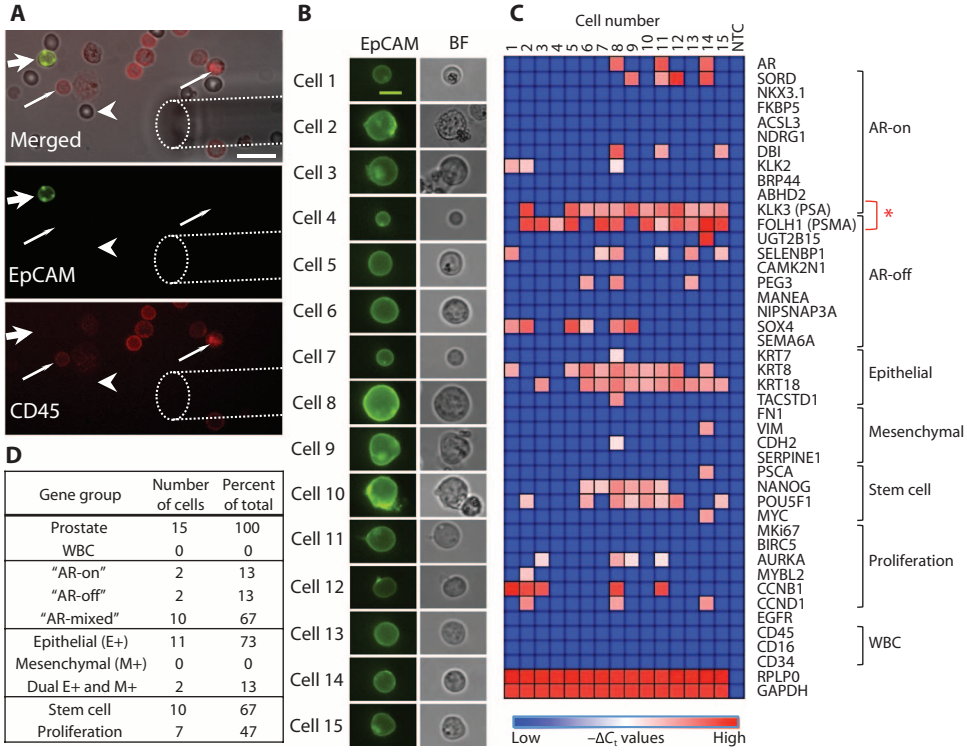

D

Gene group	Number of cells	Percent of total
Prostate	15	100
WBC	0	0
"AR-on"	2	13
"AR-off"	2	13
"AR-mixed"	10	67
Epithelial (E+)	11	73
Mesenchymal (M+)	0	0
Dual E+ and M+	2	13
Stem cell	10	67
Proliferation	7	47

Fig. 7. Heterogeneity of RNA expression between CTCs isolated from a prostate cancer patient. (**A**) Micromanipulation of single CTCs isolated from a blood specimen of a patient with prostate cancer using the ^{neg}CTC-iChip and stained in solution with anti-EpCAM (green) and anti-CD45 (red) antibodies. Top panel shows a bright-field image merged. Wide arrow points to an EpCAM$^+$/CD45$^-$ CTC. Thin arrow points to EpCAM$^-$/CD45$^+$ leukocytes. Arrowhead denotes an erythrocyte. Dashed line outlines the micromanipulator needle tip. Bottom two panels show distinct imaging channels. Scale bar, 20 μm. (**B**) EpCAM and bright-field images of 15 single prostate cancer CTCs from a single patient selected for transcriptional profiling. Scale bar, 10 μm. (**C**) Heat map of normalized gene expression ($-\Delta C_t$) of 43 genes in each of the single CTCs measured by microfluidic qRT-PCR. Columns list each individual prostate CTC, and rows show the panel of genes assayed, grouped thematically. The red asterisk highlights the gene expression patterns of PSA and PSMA, which provide a measure of AR signaling activity. NTC, no-template control. (**D**) Table listing the proportional distribution of various gene groups expressed in single CTCs isolated from the prostate cancer patient.

at high efficiency, in positive selection (tumor antigen–dependent) and negative depletion (tumor antigen–independent) modes, thus enabling cytopathological and molecular characterization of both epithelial and nonepithelial cancers. Traditional magnetophoresis requires the attachment of either hundreds of beads per cell or very large beads to provide sufficient magnetic moment for cell isolation (*11, 29*). In contrast, by virtue of its ability to precisely position cells within the channel using inertial focusing, the fluidic design of the CTC-iChip allows for efficient fractionation of cells with only a few 1-μm beads, resulting in high yields and purity of CTC isolation.

We have tested initial "proof-of-principle" clinical applications of both the positive and negative selection modes of the CTC-iChip. The ^{pos}CTC-iChip isolated CTCs at a purity of >0.1%, which is sufficient for molecular analyses, including detection of the *EML4-ALK* fusion transcript in NSCLC. Total CTC capture yield is critical to both genotyping and other applications, including enumeration for either prognostic or drug response measurements. The median number of CTCs detected by CK staining of ^{pos}CTC-iChip product was 3.2 CTCs/ml, with 90% of clinical samples having CK^+ cells above the threshold set using healthy donors. In a similar cohort using the CellSearch system, a median of 1.7 CTCs/ml was detected, with 57% of samples above the threshold (*30*). In our direct comparison between the ^{pos}CTC-iChip and the CellSearch system, the microfluidic device was significantly more sensitive at low CTC numbers (<30 CTC/7.5 ml). These results suggest that a subpopulation of $EpCAM^{low}$ cells was missed by the CellSearch bulk processing approach. Thus, whereas current commercially available approaches may be effective in patients with $EpCAM^{hi}$ CTCs, the CTC-iChip displayed increased sensitivity for patients with low numbers of circulating cancer cells, which may also have $EpCAM^{low}$ expression.

Previously, we demonstrated the efficacy of two microfluidic systems to isolate CTCs from whole blood. CK^+ CTCs were detected in 99% of patients with high purity (18 to 70%) in the first-generation micropost chip (*15*), and application of disease-specific markers for staining (PSA) and computer-assisted enumeration methods were later found to improve system reliability and specificity (*19*). Building on the improved heuristics and staining, CTCs were subsequently detected in 64% of prostate patients using the first-generation micropost chip (*19*), and in 93% of patients using the second-generation herringbone chip (*16*). Yet, these systems remain limited by low throughput (~1 to 2 ml of blood/hour), the inability to conduct single-cell or slide-based analyses, the requirement for three-dimensional image scanning platforms, and the availability of only a positive selection mode. The CTC-iChip system presented here thus encompasses major advances over our previous methods. Whole blood is now processed through a microscale system at speeds comparable to bulk systems (8 ml/hour) while preserving the high sensitivity afforded by microfluidic isolation techniques. Furthermore, rapid and gentle isolation of CTCs, as well as their collection in suspension, increases the integrity of these cells and their RNA quality, which are crucial for downstream analyses, such as cytopathology and single-cell expression profiling.

Moreover, the system can be run in either a positive selection or a negative depletion mode, thus broadening its potential application in the clinic and in basic research studies. The ^{neg}CTC-iChip allows for depletion of normal blood cells, uncovering an unselected population of nonhematopoietic cells for analysis. The robustness of this platform was demonstrated by staining CTCs per clinical pathology protocols, which yielded high-quality diagnostic images. The ^{neg}CTC-iChip allowed for isolation of CTCs from a nonepithelial cancer (melanoma) and from cancer that has undergone EMT and lost virtually all detectable EpCAM expression (triple-negative breast cancer). Hence, the ^{neg}CTC-iChip will be broadly applicable to all cancers that demonstrate vascular invasion, a major limitation of current technologies.

However, several additional optimizations should be considered before the CTC-iChip technology can be deployed for large-scale clinical applications. These include further improvements in CTC purity to facilitate routine molecular analyses of CTCs and in total blood volume processed to enable early cancer detection. From a manufacturing standpoint, we envision the CTC-iChip being integrated into a single monolithic device made of plastic and incorporating all three components of the CTC-iChip within a single footprint. Integration of such an economical chip into a fully automated device would potentially enable broad dissemination of this technology.

The emerging field of CTC biology brings with it unprecedented insight into the mechanisms underlying the blood-borne metastasis of cancer, as well as powerful new clinical applications to help diagnose and manage disease. As the technology matures, these are likely to include the initial genotyping and molecular characterization of cancer, as well as repeated noninvasive sampling of tumors during treatment. Because targeted therapies increasingly shape the clinical paradigm of cancer therapeutics, such serial "real-time" monitoring of cancer for indicators of drug response and emerging resistance is likely to become a mainstay of clinical oncology. The integrated microfluidic technology platform presented here provides a major step in this direction by enabling processing of large blood volumes with high throughput and efficiency, isolating CTCs regardless of tumor surface epitopes, and providing an end product that is compatible with both standardized clinical diagnostics and advanced molecular analyses. Because rare cell detection technologies continue to improve in sensitivity, they may ultimately provide novel approaches for early detection of invasive cancer before the establishment of metastatic disease.

MATERIALS AND METHODS

Samples

MDA-MB-231, SKBR3, and MCF10A cell lines were obtained from the American Type Culture Collection. PC3-9 cells were obtained from Veridex, LLC, and LBX1-expressing MCF10A cells were derived from a stable cell line previously published by our laboratory (*27*). Device performance was evaluated by prelabeling the cell lines with a fluorescent marker and spiking them into whole blood at ~200 to 1000/ml of whole blood (Supplementary Materials and Methods).

Fresh whole blood was collected from healthy volunteers under an Institutional Review Board (IRB)–approved protocol or commercially sourced from Research Blood Components. Samples from metastatic breast, colorectal, pancreas, lung, melanoma, and prostate cancer patients were collected under a separate IRB-approved protocol.

Chip design and fabrication

Hydrodynamic sorting chips were designed at Massachusetts General Hospital (MGH) and fabricated by Silex with deep reactive ion etching on silicon wafers. The chip was sealed with anodically bonded glass cover to form the microfluidic chamber. A custom polycarbonate manifold was used to form the fluidic connections to the microchip (fig. S3). The

inertial focusing and magnetophoresis chips were designed and fabricated at MGH with soft lithography and polydimethylsiloxane (fig. S4). The chip was placed within a custom stainless steel manifold that held four magnets in a quadrupole configuration to create a magnetic circuit enabling cell deflection (fig. S5) (Supplementary Materials and Methods).

Magnetic bead labeling of target cells in whole blood

Before processing the whole blood, samples were incubated with functionalized magnetic beads 1 μm in diameter (Dynal MyOne 656-01, Life Technologies) (fig. S2). For ^{pos}CTC-iChip, beads were functionalized with a biotinylated anti-EpCAM antibody, and active magnetic mixing was applied to achieve good labeling of EpCAM^{low} cell lines. For negative depletion, anti-CD45 and anti-CD15 functionalized beads were used (Supplementary Materials and Methods).

Immunofluorescence staining of CTCs

For enumeration analysis, isolated cells were incubated with saponin, DAPI, and anti-CK [phycoerythrin (PE)] and anti-CD45 [allophycocyanin (APC)] antibodies, acquired from Veridex, still in suspension. Cells were plated on a poly-L-lysine–functionalized glass slide with a closed chamber (fig. S8), and glass slide was scanned with the BioView imaging system while the chamber was still intact. Cells that were CK$^+$/DAPI$^+$/CD45$^-$ were scored as CTCs. Samples evaluated for PSA/PSMA expression were stained with a primary/secondary approach. All antibodies are catalogued in table S3.

Comparison to CellSearch

For the CellSearch and ^{pos}CTC-iChip comparison, two blood tubes were drawn: one CellSave tube for CellSearch run and one EDTA tube for ^{pos}CTC-iChip run. Samples in CellSave tubes were processed within 3 days after the draw as optimized and recommended for CellSearch approach, and EDTA samples were processed with the ^{pos}CTC-iChip within 4 hours of draw. CellSearch product was scanned in Magnest cartridges with CellTracks system. ^{pos}CTC-iChip product was plated and scanned with the BioView system.

RT-PCR analysis

RNA isolation was done with RNeasy Micro Kit (Qiagen). After RNA isolation, reverse transcription of RNA to complementary DNA (cDNA) using oligo(dT) was performed with SuperScript III First-Strand Synthesis System for RT-PCR (Invitrogen). For detection of *EML4-ALK* fusion cDNAs, partial nested PCR analysis was done with FideliTaq PCR Master Mix (Affymetrix). PCR amplification was performed in a thermocycler (Peltier Thermal Cycler, MJ Research). Gel electrophoresis was done with an aliquot of RT-PCR products. The amplified *EML4-ALK* products were sequenced, and results were analyzed with the ABI PRISM DNA sequence analysis software (Applied Biosystems) (Supplementary Materials and Methods).

Cytology and ICC

CTCs were enriched via ^{neg}CTC-iChip from the whole blood of cancer patients and plated on a poly-L-lysine surface (fig. S8). Plating chamber was removed after cell adhesion to facilitate standard cytopathology processing. Pap stain was done with hematoxylin, eosin-azure, and orange G and initially reviewed for suspicious cells by a certified cytotechnologist (N. Hartford, MGH) and then formally reviewed by a staff cytopathologist (E.B.). Slides were then destained and exposed to ICC process (Supplementary Materials and Methods).

Single-cell micromanipulation and qRT-PCR

Blood samples from a patient with metastatic prostate cancer were processed through the ^{neg}CTC-iChip, and unfixed CTCs and contaminating leukocytes were stained in solution with fluorophore-conjugated antibodies against EpCAM and CD45. Single CTCs were identified based on an EpCAM$^+$/CD45$^-$ phenotype and transferred under direct microscopic visualization to individual PCR tubes with a TransferMan NK2 micromanipulator (Eppendorf AG). Single-cell cDNA was prepared and amplified for single-cell transcriptome analysis, followed by specific target preamplification (Fluidigm Corp.). Microfluidic qRT-PCR was performed with the BioMark Real-Time PCR system (Fluidigm Corp.). The normalized gene expression in each cell ($-\Delta C_t$) was calculated as the negative of the difference between the C_t value for each gene and the *GAPDH* C_t value for the cell. Heat maps of normalized gene expression ($-\Delta C_t$) were generated with the Heat Map image module of GenePattern, with global color normalization.

SUPPLEMENTARY MATERIALS

www.sciencetranslationalmedicine.org/cgi/content/full/5/179/179ra47/DC1
Materials and Methods
Fig. S1. CTC-iChip system details.
Fig. S2. Optimization of labeling in whole blood.
Fig. S3. Hydrodynamic size–based separation.
Fig. S4. Inertial focusing and magnetophoresis channels.
Fig. S5. Magnetic configuration.
Fig. S6. Beads per cell distribution in deflected and undeflected outputs.
Fig. S7. WBC contamination in ^{pos}CTC-iChip.
Fig. S8. Cell plating chamber.
Fig. S9. ICC stain validation through cell lines.
Fig. S10. Additional images of ICC-stained cells.
Fig. S11. Comparison of cell identification through Pap and ICC.
Fig. S12. Single-cell qRT-PCR optimization using cell lines.
Table S1. Contaminating cells in the ^{neg}CTC-iChip product are leukocytes.
Table S2. CellSearch versus ^{pos}CTC-iChip comparison.
Table S3. Antibodies used throughout the study.

REFERENCES AND NOTES

1. K. Pantel, R. H. Brakenhoff, B. Brandt, Detection, clinical relevance and specific biological properties of disseminating tumour cells. *Nat. Rev. Cancer* **8**, 329–340 (2008).
2. M. Yu, S. Stott, M. Toner, S. Maheswaran, D. A. Haber, Circulating tumor cells: Approaches to isolation and characterization. *J. Cell Biol.* **192**, 373–382 (2011).
3. M. C. Miller, G. V. Doyle, L. W. Terstappen, Significance of circulating tumor cells detected by the cellsearch system in patients with metastatic breast colorectal and prostate cancer. *J. Oncol.* **2010**, 617421 (2010).
4. S. Maheswaran, L. V. Sequist, S. Nagrath, L. Ulkus, B. Brannigan, C. V. Collura, E. Inserra, S. Diederichs, A. J. Iafrate, D. W. Bell, S. Digumarthy, A. Muzikansky, D. Irimia, J. Settleman, R. G. Tompkins, T. J. Lynch, M. Toner, D. A. Haber, Detection of mutations in *EGFR* in circulating lung-cancer cells. *N. Engl. J. Med.* **359**, 366–377 (2008).
5. J. M. Lang, B. P. Casavant, D. J. Beebe, Circulating tumor cells: Getting more from less. *Sci. Transl. Med.* **4**, 141ps13 (2012).
6. R. T. Krivacic, A. Ladanyi, D. N. Curry, H. B. Hsieh, P. Kuhn, D. E. Bergsrud, J. F. Kepros, T. Barbera, M. Y. Ho, L. B. Chen, R. A. Lerner, R. H. Bruce, A rare-cell detector for cancer. *Proc. Natl. Acad. Sci. U.S.A.* **101**, 10501–10504 (2004).
7. D. Marrinucci, K. Bethel, A. Kolatkar, M. S. Luttgen, M. Malchiodi, F. Baehring, K. Voigt, D. Lazar, J. Nieva, L. Bazhenova, A. H. Ko, W. M. Korn, E. Schram, M. Coward, X. Yang, T. Metzner, R. Lamy, M. Honnatti, C. Yoshioka, J. Kunken, Y. Petrova, D. Sok, D. Nelson, P. Kuhn, Fluid biopsy in patients with metastatic prostate, pancreatic and breast cancers. *Phys. Biol.* **9**, 016003 (2012).
8. D. Issadore, J. Chung, H. Shao, M. Liong, A. A. Ghazani, C. M. Castro, R. Weissleder, H. Lee, Ultrasensitive clinical enumeration of rare cells ex vivo using a micro-Hall detector. *Sci. Transl. Med.* **4**, 141ra92 (2012).
9. S. Miltenyi, W. Müller, W. Weichel, A. Radbruch, High gradient magnetic cell separation with MACS. *Cytometry* **11**, 231–238 (1990).

10. G. Deng, M. Herrler, D. Burgess, E. Manna, D. Krag, J. F. Burke, Enrichment with anti-cytokeratin alone or combined with anti-EpCAM antibodies significantly increases the sensitivity for circulating tumor cell detection in metastatic breast cancer patients. *Breast Cancer Res.* **10**, R69 (2008).
11. A. H. Talasaz, A. A. Powell, D. E. Huber, J. G. Berbee, K. H. Roh, W. Yu, W. Xiao, M. M. Davis, R. F. Pease, M. N. Mindrinos, S. S. Jeffrey, R. W. Davis, Isolating highly enriched populations of circulating epithelial cells and other rare cells from blood using a magnetic sweeper device. *Proc. Natl. Acad. Sci. U.S.A.* **106**, 3970–3975 (2009).
12. R. Kalluri, R. A. Weinberg, The basics of epithelial-mesenchymal transition. *J. Clin. Invest.* **119**, 1420–1428 (2009).
13. O. Lara, X. Tong, M. Zborowski, J. J. Chalmers, Enrichment of rare cancer cells through depletion of normal cells using density and flow-through, immunomagnetic cell separation. *Exp. Hematol.* **32**, 891–904 (2004).
14. L. Yang, J. C. Lang, P. Balasubramanian, K. R. Jatana, D. Schuller, A. Agrawal, M. Zborowski, J. J. Chalmers, Optimization of an enrichment process for circulating tumor cells from the blood of head and neck cancer patients through depletion of normal cells. *Biotechnol. Bioeng.* **102**, 521–534 (2009).
15. S. Nagrath, L. V. Sequist, S. Maheswaran, D. W. Bell, D. Irimia, L. Ulkus, M. R. Smith, E. L. Kwak, S. Digumarthy, A. Muzikansky, P. Ryan, U. J. Balis, R. G. Tompkins, D. A. Haber, M. Toner, Isolation of rare circulating tumour cells in cancer patients by microchip technology. *Nature* **450**, 1235–1239 (2007).
16. S. L. Stott, C. H. Hsu, D. I. Tsukrov, M. Yu, D. T. Miyamoto, B. A. Waltman, S. M. Rothenberg, A. M. Shah, M. E. Smas, G. K. Korir, F. P. Floyd Jr., A. J. Gilman, J. B. Lord, D. Winokur, S. Springer, D. Irimia, S. Nagrath, L. V. Sequist, R. J. Lee, K. J. Isselbacher, S. Maheswaran, D. A. Haber, M. Toner, Isolation of circulating tumor cells using a microvortex-generating herringbone-chip. *Proc. Natl. Acad. Sci. U.S.A.* **107**, 18392–18397 (2010).
17. S. Wang, K. Liu, J. Liu, Z. T. F. Yu, X. Xu, L. Zhao, T. Lee, E. K. Lee, J. Reiss, Y.-K. Lee, L. W. K. Chung, J. Huang, M. Rettig, D. Seligson, K. N. Duraiswamy, C. K. Shen, H. R. Tseng, Highly efficient capture of circulating tumor cells by using nanostructured silicon substrates with integrated chaotic micromixers. *Angew. Chem. Int. Ed. Engl.* **50**, 3084–3088 (2011).
18. U. Dharmasiri, S. K. Njoroge, M. A. Witek, M. G. Adebiyi, J. W. Kamande, M. L. Hupert, F. Barany, S. A. Soper, High-throughput selection, enumeration, electrokinetic manipulation, and molecular profiling of low-abundance circulating tumor cells using a microfluidic system. *Anal. Chem.* **83**, 2301–2309 (2011).
19. S. L. Stott, R. J. Lee, S. Nagrath, M. Yu, D. T. Miyamoto, L. Ulkus, E. J. Inserra, M. Ulman, S. Springer, Z. Nakamura, A. L. Moore, D. I. Tsukrov, M. E. Kempner, D. M. Dahl, C. L. Wu, A. J. Iafrate, M. R. Smith, R. G. Tompkins, L. V. Sequist, M. Toner, D. A. Haber, S. Maheswaran, Isolation and characterization of circulating tumor cells from patients with localized and metastatic prostate cancer. *Sci. Transl. Med.* **2**, 25ra23 (2010).
20. M. Yu, A. Bardia, B. S. Wittner, S. L. Stott, M. E. Smas, D. T. Ting, S. J. Isakoff, J. C. Ciciliano, M. N. Wells, A. M. Shah, K. F. Concannon, M. C. Donaldson, L. V. Sequist, E. Brachtel, D. Sgroi, J. Baselga, S. Ramaswamy, M. Toner, D. A. Haber, S. Maheswaran, Circulating breast tumor cells exhibit dynamic changes in epithelial and mesenchymal composition. *Science* **339**, 580–584 (2013).
21. D. T. Miyamoto, R. J. Lee, S. L. Stott, D. T. Ting, B. S. Wittner, M. Ulman, M. E. Smas, J. B. Lord, B. W. Brannigan, J. Trautwein, N. H. Bander, C. L. Wu, L. V. Sequist, M. R. Smith, S. Ramaswamy, M. Toner, S. Maheswaran, D. A. Haber, Androgen receptor signaling in circulating tumor cells as a marker of hormonally responsive prostate cancer. *Cancer Discov.* **2**, 995–1003 (2012).
22. L. R. Huang, E. C. Cox, R. H. Austin, J. C. Sturm, Continuous particle separation through deterministic lateral displacement. *Science* **304**, 987–990 (2004).
23. D. Di Carlo, D. Irimia, R. G. Tompkins, M. Toner, Continuous inertial focusing, ordering, and separation of particles in microchannels. *Proc. Natl. Acad. Sci. U.S.A.* **104**, 18892–18897 (2007).
24. R. Huang, T. A. Barber, M. A. Schmidt, R. G. Tompkins, M. Toner, D. W. Bianchi, R. Kapur, W. L. Flejter, A microfluidics approach for the isolation of nucleated red blood cells (NRBCs) from the peripheral blood of pregnant women. *Prenat. Diagn.* **28**, 892–899 (2008).
25. G. Segré, A. Silberberg, Radial particle displacements in Poiseuille flow of suspensions. *Nature* **189**, 209–210 (1961).
26. A. M. Sieuwerts, J. Kraan, J. Bolt, P. van der Spoel, F. Elstrodt, M. Schutte, J. W. M. Martens, J. W. Gratama, S. Sleijfer, J. A. Foekens, Anti-epithelial cell adhesion molecule antibodies and the detection of circulating normal-like breast tumor cells. *J. Natl. Cancer Inst.* **101**, 61–66 (2009).
27. M. Yu, G. A. Smolen, J. Zhang, B. Wittner, B. J. Schott, E. Brachtel, S. Ramaswamy, S. Maheswaran, D. A. Haber, A developmentally regulated inducer of EMT, LBX1, contributes to breast cancer progression. *Genes Dev.* **23**, 1737–1742 (2009).
28. D. A. Haber, N. S. Gray, J. Baselga, The evolving war on cancer. *Cell* **145**, 19–24 (2011).
29. B. D. Plouffe, L. H. Lewis, S. K. Murthy, Computational design optimization for microfluidic magnetophoresis. *Biomicrofluidics* **5**, 13413 (2011).
30. W. J. Allard, J. Matera, M. C. Miller, M. Repollet, M. C. Connelly, C. Rao, A. G. Tibbe, J. W. Uhr, L. W. Terstappen, Tumor cells circulate in the peripheral blood of all major carcinomas but not in healthy subjects or patients with nonmalignant diseases. *Clin. Cancer Res.* **10**, 6897–6904 (2004).

Acknowledgments: We express our gratitude to all patients who participated in this study and healthy volunteers who contributed blood samples. We thank C. Koris and the MGH clinical research coordinators for help with clinical studies; B. Brannigan and H. Zhu for support of molecular analyses; E. Lim, J. Martel, J. Oakey, and F. Fachin for assistance in microfluidic device development; H. Cho for contributions to illustrations; L. Libby, O. Hurtado, and A. J. Aranyosi for coordination of the research labs; B. Hamza for expertise in device fabrication; D. Chianese and T. Bendele from Johnson & Johnson for supplying reagents and materials; and N. Bander from Weill Cornell Medical College for supplying anti-PSMA antibody, clone J591. **Funding:** This work was partially supported by NIH P41 Biotechnology Resource Center (M.T.), NIH National Institute of Biomedical Imaging and Bioengineering (M.T. and D.A.H.), Stand Up to Cancer (D.A.H., M.T., and S.M.), Howard Hughes Medical Institute (D.A.H.), Prostate Cancer Foundation and Charles Evans Foundation (D.A.H. and M.T.), Department of Defense Prostate Cancer Research Program (D.T.M. and R.J.L.), Mazzone-DF/HCC (Dana-Farber/Harvard Cancer Center) (D.T.M.), Conquer Cancer Foundation (R.J.L.), Prostate Cancer Foundation (R.J.L.), and Johnson & Johnson (M.T. and S.M.). **Author contributions:** E.O., A.M.S., B.L.E., D.T.M., E.B., M.Y., S.L.S., N.M.K., T.A.B., J.R.W., K.S., P.S.S., J.P.S., R.J.L., D.T.T., X.L., A.T.S., A.B., L.V.S., D.N.L., S.M., R.K., D.A.H., and M.T. designed the research. E.O., A.M.S., and J.C.C. were responsible for overall system design and characterization. B.L.E., A.K., and M.Y. optimized and performed cytology and ICC staining on slides. D.T.M. and J.T. executed single-cell micromanipulation and RNA analysis. S.S. conducted molecular detection of NSCLC patients. P.C., B.M., J.T., S.S., and J.C.C. executed chip operation and blood processing. N.M.K. completed characterization of cell plating chamber. E.O., P.C., and B.M. completed immunofluorescence staining, scanning, and enumeration. E.O., A.M.S., B.L.E., D.T.M., E.B., M.Y., S.L.S., N.M.K., L.V.S., S.M., R.K., D.A.H., and M.T. analyzed the research. E.O., A.M.S., B.L.E., D.T.M., S.M., R.K., D.A.H., and M.T. wrote the paper. **Competing interests:** MGH filed for patent protection for the CTC-iChip technology. The authors declare that they have no competing interests. **Data and materials availability:** Biotinylated anti-EpCAM mouse monoclonal IgG1 (clone VU-1D9), PE-conjugated anti-CK8/18 mouse monoclonal IgG1 (clone C11), PE-conjugated anti-CK19 mouse monoclonal IgG2a (clone A53-B/A2), APC-conjugated anti-CD45 mouse monoclonal IgG1 (clone HI30), nuclear staining reagent DAPI, and cell membrane permeabilization reagent saponin were obtained under a Materials Transfer Agreement from Johnson & Johnson (contact: David Chianese). Anti-PSMA monoclonal mouse IgG1 antibody (clone J591) was obtained under Materials Transfer Agreement from Weill Medical College (contact: Neil Bander).

Submitted 27 August 2012
Accepted 22 March 2013
Published 3 April 2013
10.1126/scitranslmed.3005616

Citation: E. Ozkumur, A. M. Shah, J. C. Ciciliano, B. L. Emmink, D. T. Miyamoto, E. Brachtel, M. Yu, P. Chen, B. Morgan, J. Trautwein, A. Kimura, S. Sengupta, S. L. Stott, N. M. Karabacak, T. A. Barber, J. R. Walsh, K. Smith, P. S. Spuhler, J. P. Sullivan, R. J. Lee, D. T. Ting, X. Luo, A. T. Shaw, A. Bardia, L. V. Sequist, D. N. Louis, S. Maheswaran, R. Kapur, D. A. Haber, M. Toner, Inertial focusing for tumor antigen–dependent and –independent sorting of rare circulating tumor cells. *Sci. Transl. Med.* **5**, 179ra47 (2013).